A critical review of direct laser additive manufacturing ceramics

Dake Zhao[1,2], Guijun Bi[1,2]*, Jie Chen[1,2], Wai-Meng Quach[3], Ran Feng[4], Antti Salminen[5]

1) Institute of Intelligent Manufacturing, Guangdong Academy of Sciences, Guangzhou, 510070, China

2) Guangdong Key Laboratory of Modern Control Technology, Guangzhou, 510070, China

3) Department of Civil and Environmental Engineering, University of Macau, Macau, China

4) School of Civil and Environmental Engineering, Harbin Institute of Technology, Shenzhen, 518055, China

5) Department of Mechanical and Materials Engineering, Faculty of Technology, University of Turku, FI-20014 Turun yliopisto, Finland

* Corresponding author: Guijun Bi. E-mail: gj.bi@giim.ac.cn

Abstract: The urgent need for integrated molding and sintering across various industries has inspired the development of additive manufacturing (AM) ceramics. Among the different AM technologies, direct laser additive manufacturing (LAM) stands out as a group of highly promising technology for flexibly manufacturing ceramics without molds and adhesives in a single step. Over the last decade, significant and encouraging progress has been accomplished in direct LAM of high-performance ceramics, including Al_2O_3, ZrO_2, Al_2O_3/ZrO_2, SiC, and others. However, high-performance ceramics directly fabricated by LAM face challenges such as formation of pores and cracks and resultant low mechanical properties, hindering their practical application in high-end equipment. Further improvements are necessary before they can be widely adopted. Methods such as field-assisted techniques and post-processing can be employed to address these challenges, but a more systematic review is needed. This work aims to critically review the advancements in selective laser sintering/melting (SLS/SLM) and laser directed energy deposition (LDED) for various ceramic material systems. Additionally, it provides an overview of the current challenges, future research opportunities, and potential applications associated with direct LAM of high-performance ceramics.

Keywords: 3D printing; Laser additive manufacturing; Ceramics; Quality; Microstructure; Mechanical properties

1 Introduction

Diverse industries continuously favor high-performance ceramic parts for their exciting properties in extreme and severe environments, such as high temperatures resistance, outstanding corrosion and erosion resistance, and excellent wear resistance. The substitution of superalloys with ceramics can objectively reduce the weight of critical core parts, promising to enhance the agility and maneuverability of aircraft [1]. Furthermore, the exceptional heat resistance of ceramics promotes combustion efficiency in internal combustion engines (ICE) and turbomachinery, leading to reduced carbon emissions. Ceramics also excel in handling the energy field, such as in the nuclear industry, where aggressive corrosion and high radiation fluxes are prevalent [2]. These high-value ceramic parts encompass exhaust nozzle, combustor liner, turbine blade, vane, molten salt reactor (MSR), catalytic converter, and EV bearing [3]. Therefore, the judicious utilization of ceramic parts is anticipated to achieve long-awaited goals of increased efficiency, enhanced performance, and extended lifespan of high-end equipment. This is particularly pertinent given the rising emphasis on low emissions.

However, achieving the desired geometry and surface finish using conventional manufacturing processes to produce ceramic parts, such as shaping and sintering, involves multiple steps with long cycles, including material preparation, processing, sintering, heat treatment, and finishing [4]. Direct laser additive manufacturing (LAM) provides the possibility for single-step shaping of complex near net shape ceramic parts, and generally have two main variants depending on the powder feeding mode: selective laser sintering/melting (SLS/SLM) and laser directed energy deposition (LDED). The LDED process has been developed independently by different research teams around the world, giving rise to different acronymic terms, such as laser engineered net shaping (LENS), laser metal deposition (LMD), direct metal deposition (DMD), and directed laser deposition (DLD), etc. [5]. In fabrication of a ceramic part by direct LAM, a laser beam is used to transform the 3D design of the part into a complete solid in a rational manufacturing path. The ceramic parts are formed by sintering or solidifying in a layer-by-layer manner. As a result, these techniques demonstrate many advantages: (i) single step moldless manufacturing of near net shape ceramic parts; (ii) flexible design of structures and materials; (iii) low-volume and high-precision production capabilities; and (iv) easy fulfillment of quick-response and short-cycle manufacturing requirements. Research on the topics of ‘ceramic’ using the LAM processes has attracted worldwide attention and investment over the last two decades, with the number of publications

increasing over time, as illustrated in **Fig. 1(a)**. The number of studies on the LAM processes of critical topics for some typical ceramics during this period is shown in **Fig. 1(b)**. It can be seen that the research involving Al_2O_3 has received more attention. Moreover, a research report by SmarTech Analysis shows that the additive manufacturing market for ceramics will reach $400 million by 2032 [6], further encouraging the careful study of high-performance ceramics by direct LAM processes.

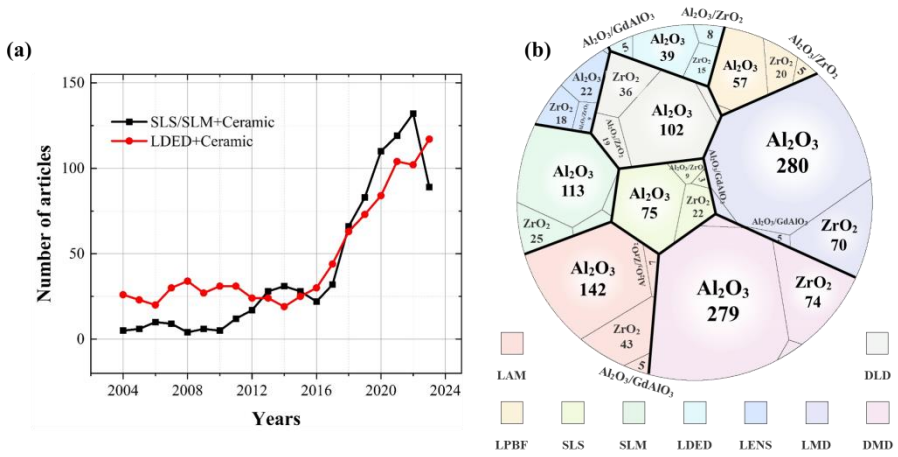

Fig. 1. Number of articles involved in 'Core collection databases' on 'Web of Science' with the topics 'ceramic' and 'Selective Laser Sintering/Melting' or 'Laser Directed Energy Deposition' (a); as well as the 'LAM processes' (abbreviated as 'LAM', 'LPBF', 'SLS', 'SLM', 'LDED', 'LENS', 'LMD', and 'DLD') and 'typical ceramics' (relate to 'Al_2O_3', 'ZrO_2', 'Al_2O_3/ZrO_2', and '$Al_2O_3/GdAlO_3$') (b) till 31th of December 2023.

The quality and properties are prerequisites for AMed ceramic parts to withstand various harsh conditions, typically influenced by multiple parameters of the LAM processes within the domain-by-domain and layer-by-layer shaping characteristics. These parameters include laser power (*P*), scanning speed (*v*), closely linked to solidification rate (*R*), powder bed density, powder feed rate (*m*), scan pattern, hatch spacing (overlap rate), and processing atmosphere environment. The quality of directly LAMed ceramic parts encompasses defects, residual stresses, inclusions, geometric accuracy, and surface roughness, among others. The processing parameters significantly influence the shape and size of the smallest unit in continuous shaping part: a partial melting microfluid [7] or a fully melted melt pool. The thermal and mass history of the LAM process is complex and influenced by numerous parameters, which are the main factors for direct LAM of high-quality parts. On one hand, regulating the thermal history homogenizes and refines the microstructure, guaranteeing material properties. On the other hand, efficient diffusion

and convective transportation of matter (mass history), such as powder delivered to the melt pool and microfluid in the melt pool, are essential for manufacturing low-defect high-precision parts. However, the multiple processing parameters and extremely high-temperature pose significant challenges to high-performance ceramic parts by controlling the thermal and mass history.

Several publications cover direct LAM processes for high-performance ceramics [8-10]. However, as of this writing, there are few careful reviews of the parts quality for direct LAM ceramics. The existing reviews on the correlation of defects, structures, and properties with process parameters need to be supplemented, especially the paucity of reviews dealing with the effects of external field-assisted shaping and post-treatment. Consequently, with a brief overview of the process principles (Section 2), this review article scrutinizes the progress in shaping quality (Section 3), microstructure (Section 4), and mechanical properties (Section 5) of direct LAM ceramics, contributing positively to further academic research and potential industrial development. Furthermore, this review also prospects future opportunities and potential applications of direct LAMed high-quality ceramics, such as large-size, crack-free, high density, high accuracy, and high properties.

2 Process principles of direct LAM ceramics

2.1 Selective laser sintering/melting

The selective laser sintering (SLS) process traces its origins to a patent filed by Carl R. Deckard in 1980, which outlined the fundamental principles of combining the SLS process with subsequent patents. In this process, the powder is initially spread flat on a powder bed and then subjected to a laser beam following a predefined trajectory. This is followed by downward movement of the powder bed to create a layer. This sequence is repeated to realize the manufacturing of complex shape parts, as shown in **Fig. 2(a)**. Similarly, the principle behind the selective laser melting (SLM) process is akin to the SLS process, with the distinction that the SLM process operates at temperatures exceeding the melting point of the additive material to produce dense parts. The SLM process originated as a research project at the Fraunhofer ILT in Aachen, Germany. Recent years have witnessed a gradual increase in research focused on SLMed ceramics, driven by the demand for single-step processing of dense ceramics.

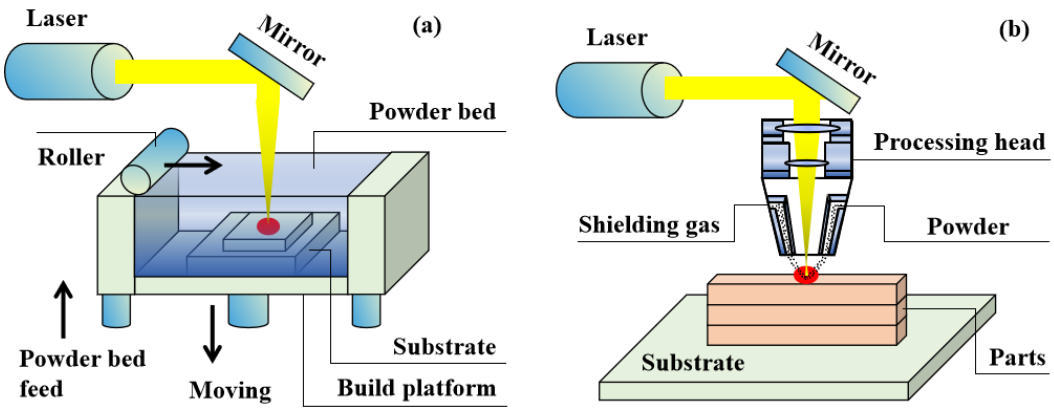

Fig. 2. Schematics of the direct laser additive manufacturing: (a) selective laser sintering/melting processes; (b) laser directed energy deposition process.

2.2 Laser directed energy deposition

LDED process synchronizes laser radiation and powder feeding, as shown in **Fig. 2 (b)**. This process involves converging spherical ceramic powders onto the substrate using a powder feeder and a nozzle. Simultaneously, a high-energy laser beam creates a melt pool on the substrate, melting the powders, followed by rapid cooling. By coordinating the relative movement between the processing head and the substrate according to a path pattern formed by layered slicing, a final three-dimensional part can be fabricated. Various ceramic materials have been developed for single-step direct LAM, as shown in **Table 1**, illustrating the significant potential of the direct LAM processes (SLS/SLM and LDED) for the single-step manufacturing of high-quality advanced ceramics.

Table 1 Summary of ceramic materials available for the LAM processes

Process	Ceramic materials
SLS/SLM	Al_2O_3 [11-13], ZrO_2 [14-16], SiC [17], SiO_2/glass [18, 19], Y_2O_3 [20], $BaTiO_3$ [21], High-entropy carbide ceramics [22], Al_2O_3/ZrO_2 [23-25], $Al_2O_3/GdAlO_3$ [26], $Al_2O_3/GdAlO_3/ZrO_2$ [27]
LDED	Al_2O_3 [28, 29], ZrO_2 [30], $MgAl_2O_4$ [31], Mullite [32], Al_2O_3/ZrO_2 [33-38], Al_2O_3/Al_2TiO_5 [39], $Al_2O_3/GdAlO_3/ZrO_2$ [40], Al_2O_3/YAG/ZrO_2 [41], Al_2O_3/YAG [42], Al_2O_3/mullite [43]

3 Quality of directly LAMed ceramics

Manufacturing high-performance ceramic parts in a single step using the LAM processes is not an effortless task, particularly when facing the urgent demands for large-size and crack-free. The LAM physical process for ceramics is characterized by complexity and extremity due to the brittle nature and high melting point, encountering

numerous processing variables. Hence, ensuring the quality of LAMed ceramics is an exciting and critical research topic. This section summarizes the geometric properties and surface roughness of ceramic parts fabricated by the LAM processes. In addition, the defect inhibition methods are also reviewed carefully.

3.1 Geometric properties

Geometric dimensions and accuracy, are direct indications of the capability of the LAM processes to fabricate high-performance ceramic parts, which has been the focus of numerous studies. **Table 2** provides a detailed summary of research on these factors. The SLS/SLM processes, with solid sintering or partial melting features, are recognized for their ability to fabricate complex shape ceramics. However, they often yield low densities and surface roughness. For instance, the maximum transverse section dimensions (width) of SLS/SLMed Al_2O_3 parts with different shapes and widths of 67.8 mm were fabricated by adding small amounts of graphite [11], as shown in **Fig. 3(a)**, but these structures are damaged at the microscopic level. In addition, direct printing of high geometric accuracy parts is usually at the expense of densification. Similar findings have been observed for pure ZrO_2 parts, including turbine blade, wall, and cube [16], which was considered to have an accurate geometry compared to the CAD design [44], but only 56% density. Numerical simulation-guided process optimization enables the manufacturing of SiC parts with a width of 20 mm [45] (**Fig. 3(b-c)**). Regranulation appears to be a viable approach for fabricating large-size and complex-shape parts, such as SLS/SLMed Al_2O_3/ZrO_2 ceramics with a width of about 41 mm and poor surface roughness [24] (**Fig. 3(d)**). In contrast, due to the thermal stresses, the SLS/SLM processes with fully melting features require high-temperature preheating to produce fully structured parts. Typical representatives are Al_2O_3/ZrO_2 ceramics with a width of 31-41mm [23], such as frameworks for dental restoration and turbines for turbochargers (**Fig. 3(e)**). The SLMed $Al_2O_3/GdAlO_3/ZrO_2$ ternary eutectic ceramics with different shapes aided by finite element analysis (FEA) shows a width of 30 mm [46] (**Fig. 3(f)**). The results also show that ceramic structures with curved or rounded edges have a higher crack formation tolerance and the part is considered to have good geometric accuracy.

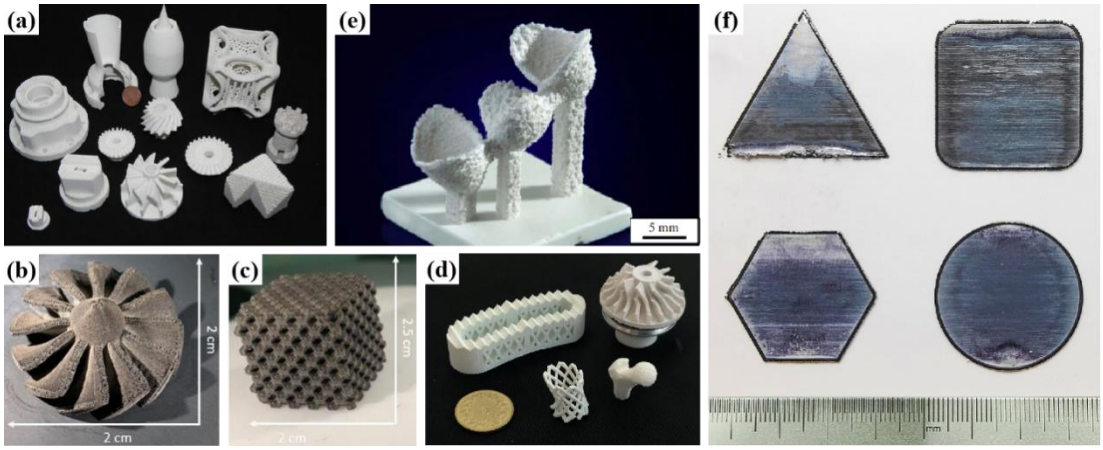

Fig. 3 Typical ceramic parts fabricated by SLS/SLM processes: (a) Al_2O_3 ceramics [11], (b) and (c) SiC ceramics [45], (d) and (e) Al_2O_3/ZrO_2 ceramics [23, 24], (f) $Al_2O_3/GdAlO_3/ZrO_2$ eutectic ceramics [46].

Table 2 Geometric properties of typical ceramic structures fabricated by the LAM processes

Process	Materials	Geometric shape	Geometric dimensions[#]		Geometric accuracy
			Width[*] (mm)	Height[*] (mm)	
SLS/SLM	Al_2O_3 [11]	Turbine, lattice, hollow, and end cap structures	~67.8	~81.3	Good accuracy with lower-density
SLS/SLM	Al_2O_3 [47]	Thin sheet with cracks	~10	~0.5	lower *v* reduces shaping accuracy
SLS/SLM	Al_2O_3 [13]	Thin-walled structure	~10	~0.5	N/A
LDED	Al_2O_3 [28]	Gear, stepped discoidal structure, cylinder, cube	~25	~33	N/A
LDED	Al_2O_3 [29]	Cylinder	~5	≥200	N/A
SLS/SLM	Al_2O_3/ZrO_2 [24]	Turbine, hollow structure	~41.4	~8.1	N/A
SLS/SLM	Al_2O_3/ZrO_2 [23]	Turbine, framework	~41.4	~19.4	N/A
LDED	Al_2O_3/ZrO_2 [33]	Arc wall, cylinder	~19	~52	N/A
LDED	Al_2O_3/ZrO_2 [48]	Cylinder	~5	~230	N/A
SLS/SLM	SiC [45]	Turbine	~20	~20	N/A
		Lattice structure	~20	~25	
SLS/SLM	ZrO_2 [14]	Turbine	~30	N/A	Relatively good accuracy
SLS/SLM	ZrO_2 [15]	Rectangular sheet	~25	~3-3.75	Fulfills the CAD design basically
LDED	Al_2O_3/Al_2TiO_5 [49]	Cylinder	~5	~200	N/A
		Thin-walled rings	~15	~20	
SLS/SLM	$Al_2O_3/GdAlO_3/ZrO_2$ [46]	Triangular prism, hexagonal prisms, cylinders, cubic	~30	~1	Good accuracy
LDED	$Al_2O_3/GdAlO_3/ZrO_2$ [40]	Cylinder	~5	~410	N/A
		Corner shape	~8	~64	

[#] Geometric dimensions mean the achievable section dimension in the publications.

[*] Width = Transverse section dimension, High = Longitudinal section dimension.

The LDEDed Al_3O_3 gear and cylinder [28], as listed in **Table 2**, have a width of 10-25 mm, as shown in **Fig. 4(a)**. Al_2O_3/ZrO_2 eutectic ceramics formed by ZrO_2 doping with arc wall and cylinder shapes have a width of less than 18 mm [33] (**Fig. 4(b)**). When the width is narrow (less than 6 mm), crack-free structures can be freely fabricated in the build direction (or deposition direction, *Z*-axis), mainly limited by the machine threshold (Fig. 4(c-d)) [48, 49]. This argument is supported by the investigations of Liu [40], which show a height dimension of about 410 mm, as shown in **Fig. 4 (e)**. Corner-shaped structures with a width of about 8 mm can be built by adjusting the scanning strategy after process optimization, considered to have a good geometric accuracy. Therefore, the dimension in the build direction of LDEDed crack-free ceramics appears to be unrestricted, but the dimension in the vertical build direction is significantly limited due to tensile stress. An investigation of Al_2O_3 ceramics demonstrated the critical effect of process parameters on the geometric properties of LDEDed parts [50]. This study believes that an increase in *P* has a positive effect on the length of the printed single track, with a slight change in width. The rise in *v* deteriorates the dimension accuracy, associated with less powder entering the melt pool. However, considering the design size (Φ4 mm), the geometric accuracy of LDEDed mullite cylinders may be poor (Φ5~6 mm) [51]. Further analysis suggests that this may be related to poor-quality deposition layers due to the high viscosity of the rapidly cooled silica-containing melt pool. Numerical simulation of the melt flow during LAM of ceramics may be helpful.

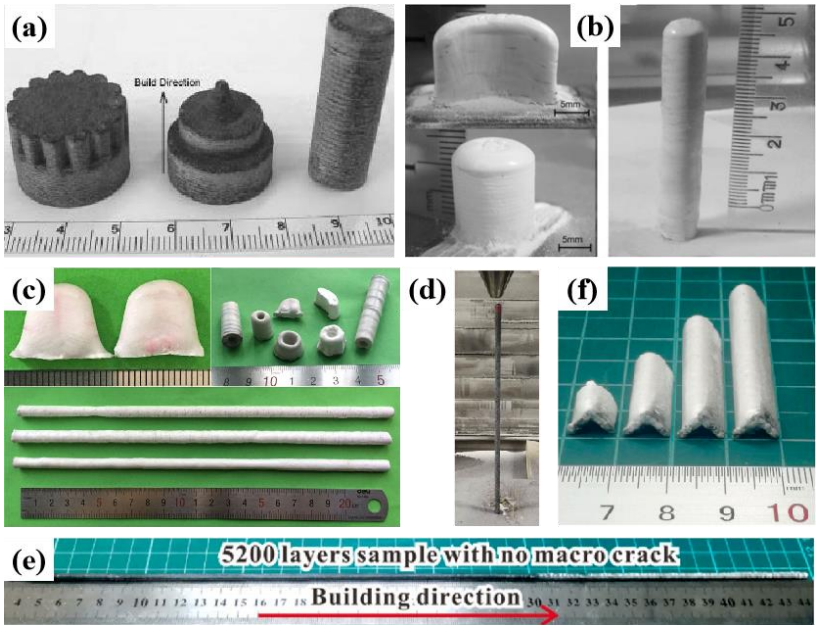

Fig. 4 Typical ceramic parts fabricated by LDED processes: (a) Al_2O_3 ceramics [28], (b) Al_2O_3/ZrO_2 eutectic ceramics [33], (c) Al_2O_3/ZrO_2 ceramics [48], (d) Al_2O_3/Al_2TiO_5 ceramics [49], (e) and (f) $Al_2O_3/GdAlO_3/ZrO_2$ eutectic ceramics [40].

3.2 Surface roughness

Surface roughness (R_a) is a critical parameter for evaluating part quality, referring to the degree of unevenness in the micro peaks and valleys on the part surface [52]. **Table 3** presents an investigation of R_a for LAMed ceramics. The R_a of SLS/SLMed SiO_2 and $ZrSiO_4$ ceramics increases with increasing P and decreases with increasing v, as concluded by Klocke [53] and Tang [54]. This pattern of change was also found in the investigation of Al_2O_3 parts, where Fayed [12] concluded that the increase in laser energy density (LED, $Q = P/v$ or P/vm) leads to the formation of larger-sized spherical structures, increasing R_a. On the other hand, an increase in v reduces the possibility of plasma formation, which increases the R_a. Hagedorn [55] believes that reducing the particle size in the powder bed can further improve the R_a of Al_2O_3/ZrO_2 parts. Furthermore, the influence law of v on R_a was also observed by Shen [46]. The scanning strategy is also considered one factor affecting the R_a of LAMed ceramics, and the linear-45° strategy had the lowest R_a of 97 μm [56]. Optimizing the defocusing distances is another strategy to modulate the R_a of SLS/SLMed ceramics. Xiong [57] argues that with the increase of defocusing distance, the R_a follows a pattern of first decreasing and then increasing. Moreover, other factors that affect the R_a of the part are adhesion of unmelted particles [50], lumps [58], and wettability. As for LDED of ceramics, Li conducted a detailed investigation of the R_a abut LDEDed Al_2O_3 block parts [50]. The results indicate that the R_a gradually decreases with the increase of P and powder feed rate (m), and first decreases and then increases with the rise of v, which may be related to the energy input to the melt pool and the degree of powder melting. For LDEDed Al_2O_3 ceramics, Mishra [59] concluded that as the P is increased from 225 W to 300 W, the surface morphology of a single track will gradually evolve from unformed (low P) to smooth (high P), that is, the R_a gradually decreases. Also, laser remelting is another method to improve the R_a of LAMed ceramics [24].

Table 3 Studies on surface roughness in LAM-processed ceramics

Author	Process	Main features
Tang [54]	SLS/SLM	Increase P, R_a increases from 21.8 μm to 30 μm Increase v, R_a decreases from 34.1 μm to 18.7 μm

Fayed [12]	SLS/SLM	Increasing *P* and/or decreasing *v* leads to an increase in R_a, ranging from 0.5 μm to 2.7 μm
Abdelmoula [56]	SLS/SLM	Scanning strategy significantly affects R_a Linear-45° pattern shows a low R_a of 90 μm, and island-concentric shows a high R_a of 206 μm
Hagedorn [55]	SLS/SLM	Preheated LAM deteriorates the R_a (150 μm), and decreasing powder particles improves the R_a
Shen [46]	SLS/SLM	R_a can be reduced by increasing the *v* (from 7.332 μm to 3.377 μm)
Xiong [57]	SLS/SLM	R_a decreases first and then increases (from 9.2 μm to 6.05 μm, and 6.05 μm to 9.5 μm) when the defocusing distance increases from -3mm to 3mm
Li [50]	LDED	Increase *P* and powder feed rate, R_a decreases from 9.1 μm to 6.4 μm and 7.4 μm to 5.3 μm. Increase *v*, R_a increases from 4.6μm to 7.3 μm
Liu [60]	LDED	R_a increases from 0.13-0.18 μm to 0.65 μm with increasing annealing temperature

3.3 Defects

Defects play a critical role in determining the mechanical properties and performance of LAMed ceramics. This section provides an overview of defect characterization and inhibition methods for ceramics fabricated through LAM processes. Detailed information is summarized in **Table 4**.

3.3.1 Cracks

Cracking is the primary challenge in LAMed ceramics due to strong crack sensitivity. Crack formation is generally considered to be caused by the shrinkage, thermal shock, and/or thermal stress in the parts during sintering or melting [11]. The morphology of poorly dense parts with cracks and deeper cracks in SLS/SLMed ceramics is shown in **Fig. 5(a-b)**. Morphologically, several studies have concluded that cracks in LAMed ceramics can be categorized into two types: longitudinal cracks and transverse cracks (**Fig. (c-e)**) [61, 62]. The longitudinal cracks that usually form are more severe than the transverse cracks. Consequently, the influence of longitudinal cracks on quality is more significant. A combination of powder bed conditions, internal pores, and thermal stresses may be responsible for the formation and propagation of the two types cracks [63]. Inappropriate selection of powder bed density will lead to the

formation of defects between the melt tracks due to insufficient melt, increasing the susceptibility to transverse crack formation [47]. Correspondingly, the origin of longitudinal cracks may be related to the vaporization hole generated at the beginning of printing [62]. Alternatively, the non-uniform distribution of laser energy leading to the non-uniform thermal stresses may also be a reason for forming these ordered longitudinal cracks.

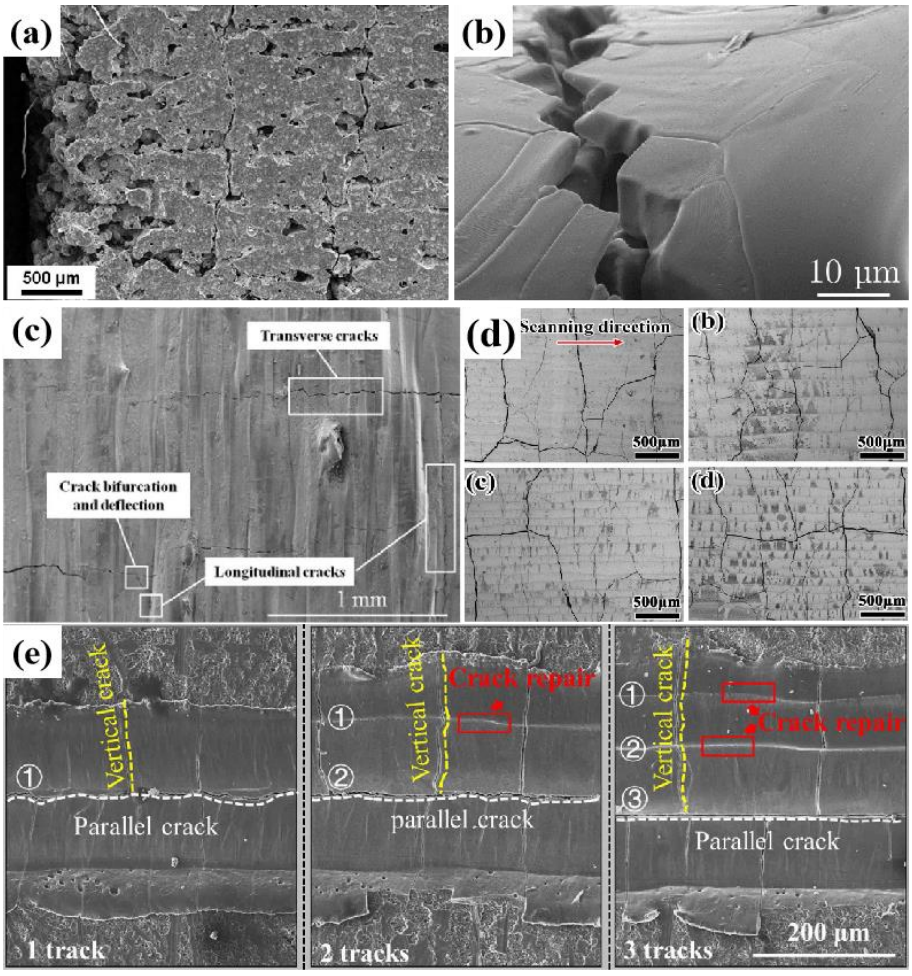

Fig. 5 Cracking characteristics of the SLS/SLM-processed ceramics: (a) [11], (b) [64], and (c) [62] Al_2O_3 ceramics, (d) Al_2O_3/$GdAlO_3$/ZrO_2 eutectic ceramics [46], (e) Al_2O_3/ZrO_2 eutectic ceramics [25].

LDEDed ceramics seem more prone to cracking than SLS/SLM due to higher thermal stresses [28]. Similar crack morphologies, longitudinal and transverse cracks, have also been found in LDEDed ceramics, as reported by Niu [61], and shown in **Fig. 6(a)**. In their case, the surface cracking of thin-walled structures in the printed state was relatively severe, and similar findings were found in printing Al_2O_3/ZrO_2 [48], Al_2O_3/TiO_2 [65], and magnesium aluminate spinel [31]. For longitudinal cracks parallel to the build direction, cracking research for Al_2O_3 ceramics [28] suggested that thermal

stresses and strain discontinuities between adjoining deposited layers were responsible for forming intergranular longitudinal cracks. However, due to the complex thermal history and the built structure, thermal stress between adjacent layers does not seem to explain the formation of longitudinal cracks [66] thoroughly. For example, LDEDed mullite has shown that longitudinal cracks can be caused by air pores at the sample bottom and shrinkage cavities at the sample top [32], also found by Su [40], as shown in **Fig. 6(b)**. Consequently, cracking of LAMed ceramics from the bottom seems to be a high probability occurrence, resulting in longitudinal cracks with secondary for transverse cracks in severe circumstances (**Fig. 6(c)**). Therefore, numerical simulation combined with the thermal performance of ceramics for the detailed heat and stress distribution of the LAM processes is necessary to clarify the crack initiation mechanism and propose practical inhibition approaches.

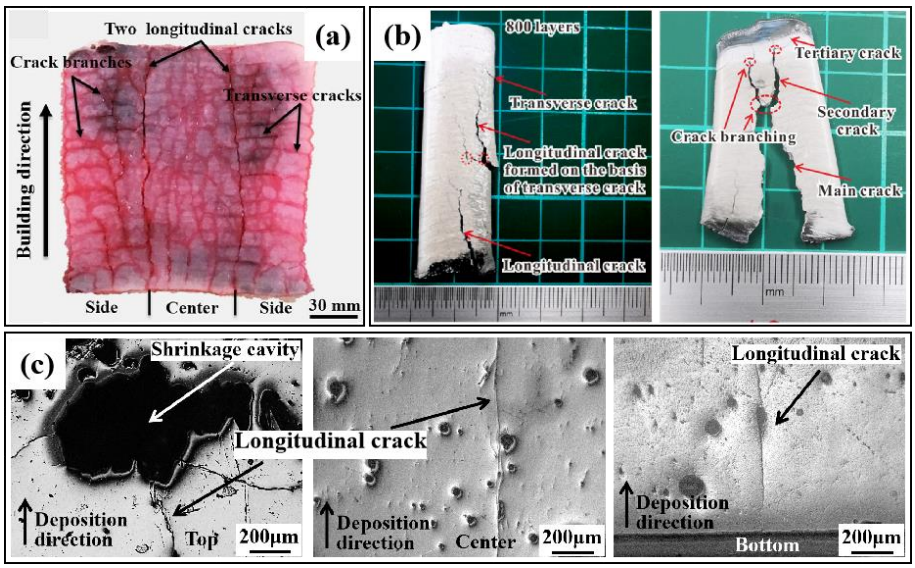

Fig. 6 Characteristics of cracks in LDED-processed ceramics: (a) Al_2O_3/ZrO_2 ceramics [48], (b) $Al_2O_3/GdAlO_3/ZrO_2$ eutectic ceramics [40], (c) mullite [32].

3.3.2 Voids

Void is another critical factor affecting the property and performance of LAMed ceramics. However, avoiding void formation is challenging, especially for deposition of ceramics [66]. There are several types of voids, such as poorly bonded voids, lack of fusion, and air pores, as shown in **Fig. 7**. Poorly bonded voids are common in SLS/SLMed parts and result from the solid sintering or partial melting (**Fig. 7(a)**) [44]. Insufficient laser intensity, uneven laser energy distribution, or inappropriate processing parameters in the SLS/SLM and LDED processed can lead to inadequate liquid phase into the solidified layer, forming a lack fusion (**Fig. 7(b)**). The shrinkage

band distributed on top of LDEDed parts is a type of lack of fusion formed by merging a series of shrinkage cavities (**Fig. 7(a)**). Shrinkage cavities are usually created by the failure of the liquid to fill the gap because of the rapid solidification at the top part, which can be removed by further laser remelting. Air pores are prevalent in LAMed ceramics [67]. Specifically, bubble nuclei, due to the low solubility of gases, float, merge, and grow under driving forces (e.g., buoyancy and surface tension), similar to those found in casting or welding [68], failing to escape from the rapidly solidifying melt pool and forming air pores. Furthermore, the primary gas sources are surface entrainment, internal carryover of powders, and evaporation of low melting point substances [36]. The complete voids morphology and distribution inside LAMed ceramics can be obtained by the synchrotron-based X-ray micro-computed tomography (SR-μCT) [59] and deep-learning-based porosity analysis method [69], which give exciting fabrication and post-processing methods to scrutinize the voids formation and distribution of deposited ceramics. As a result, LDEDed parts have lower voids than SLS/SLMed with solid sintering or partial melting, with densities above 95%, due to the full melting bond mechanism.

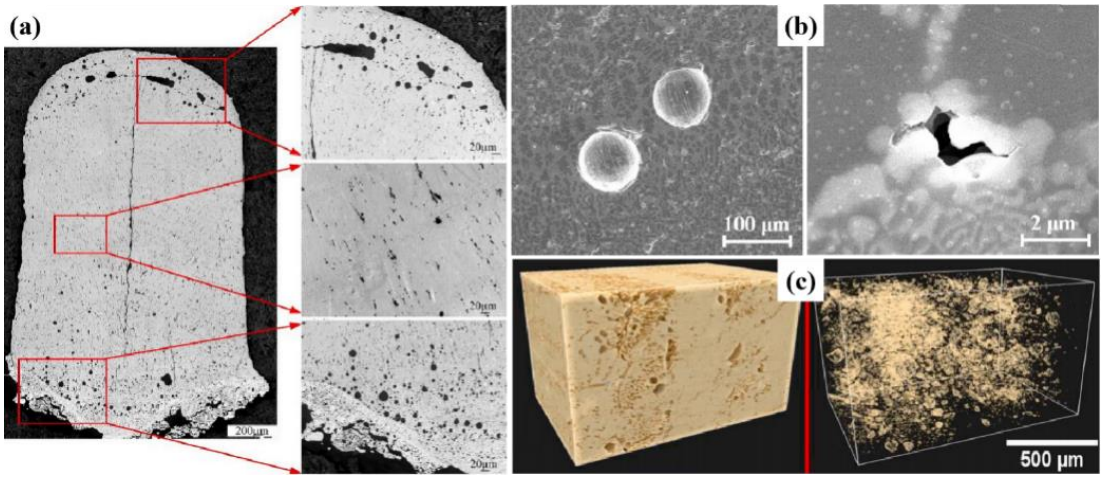

Fig. 7 Characteristics of voids in LAM-processed ceramics: (a) Al_2O_3/ZrO_2 ceramics [66], (b) Al_2O_3/ZrO_2 eutectic ceramics [36], (c) Al_2O_3 ceramics [59].

Table 4 Defect characteristics and relative density of ceramics fabricated by the LAM processes

Author	Materials	Processes	ρ (%)	Defect characteristics and formation mechanism	Process for low-defect parts
Deckers [64]	Al_2O_3	SLS/SLM	85	Cracks: stop at the solidified surface end, resulting from thermal deformation (curling) Voids: distributed between microstructures, caused by incomplete melting	P = 2 W, v = 5.2 mm/s
Juste [11]	Al_2O_3	SLS/SLM	> 90	Cracks: thermal shocks and/or thermal stresses induced by a heterogeneous sintering Voids: a consequence of stacking defects in the powder bed	Q = 16.6 J/mm²
Balla [28]	Al_2O_3	LDED	94	Crack-free, cracking caused by thermal stresses when the process is not appropriate Voids: low energy densities for highly porous ceramics caused by incomplete melting	P = 175 W, v = 10 mm/s
Niu [29]	Al_2O_3	LDED	99.5	Cracks: crack-free Voids: small spherical pores, formed by decreased solubility of gases. Large ellipsoidal pores are formed by agglomeration of small pores	P = 375 W, v = 300 mm/min
Mishra [59]	Al_2O_3	LDED	≤ 95	Cracks: appeared after printing of six layers Voids: distributed at different locations on the part	P = 300 W, v = 0.6 mm/min.
Liu [70]	ZrO_2	SLS/SLM	84-91	Cracks: vertical ordered crack and crossing crack Voids: small pores evolve into large pores, which rupture to form cracks	Preheating above 1500 °C
Ferrage [15]	ZrO_2	SLS/SLM	96.5	Cracks and voids: cracks are present between the columns and the pores are 1 μm	P = 84 W, v = 70 mm/s
Fan [30]	ZrO_2	LDED	98.7	Crack: vertical and horizontal cracks	P = 325 W, v = 355 mm/min
Abdelmoula [17]	SiC	SLS/SLM	87	Voids: high porosity, powder not fully melting. Layer degradation and decomposition	P = 45 W, v = 100 mm/s
Zhang [22]	high-entropy carbide	SLS/SLM	> 99	Cracks: free-crack Voids: free-pore	P = 300-600 W, v = 0.22 mm/s
Pappas [31]	$MgAl_2O_4$	LDED	98	Crack length and pores increase with increasing P	P = 275 W, v = 0.7 mm/min
Wu [51]	Mullite	LDED	97.8	Cracks: distributed in the sample center Voids: large pores are distributed at the sample edge	P = 300 W, v = 200 mm/min
Wilkes [23]	Al_2O_3/ZrO_2	SLS/SLM	~100	Cracks: small parallel cracks	Preheat the powder bed to 1600 °C
Verga [24]	Al_2O_3/ZrO_2	SLS/SLM	96	Cracks: cracks smaller than 1 μm in thickness and several micrometers in length	N_2 shielding atmosphere
Ma [71]	Al_2O_3/ZrO_2	LDED	98.3	Cracks and cavities are distributed in the cellular structure boundaries	P = 530 W, v = 400 mm/min

Yan [72]	Al_2O_3/ZrO_2	LDED	N/A	Crack: longitudinal crack in the bottom center, transverse crack in the middle edge Voids: spherical air pore and irregular shrinkage cavity	Ultrasound-assisted, 120 W
Pappas [38]	Al_2O_3/ZrO_2	LDED	~ 97	Crack: expand in both transverse and longitudinal directions Voids: porosity increases with increasing ZrO_2 content	Add 10 wt% ZrO_2
Huang [49]	Al_2O_3/Al_2TiO_5	LDED	98	Cracks: several branched longitudinal dendritic cracks at low *v* Voids: small pores are distributed inside the sample	Rapid scanning, 900 mm/min
Zhao [43]	Al_2O_3/mullite	LDED	≤ 99.4	Cracks: multiple transverse cracks and some longitudinal cracks Voids: small pore morphology distributed inside samples with low Al_2O_3 content	*P* = 275 W, *v* = 0.7 mm/min
Shen	$Al_2O_3/GdAlO_3/ZrO_2$	SLS/SLM	N/A	Cracks: transverse and longitudinal cracks, formed by tensile and shearing stress Voids: small-size pores at the track center, and large-size pores at the track edge	*P* = 300 W, *v* = 300 mm/s Finite element analysis
Liu	$Al_2O_3/GdAlO_3/ZrO_2$	LDED	98.7	Cracks: large cracks form when deposited layers increase to 100	Preheating substrate, shortening scan length, and laser remelting

3.3.3 Inhibition approaches

Many approaches have been investigated to fabricate dense and crack-free ceramics, including process optimization, preheating powder bed or substrate, ultrasound-assistance, adding enhancement phases, and laser remelting as listed in **Table 4.** Process optimization was a preferred and easy method to inhibit defects. However, the SLSed ceramic parts with complex-shape were insufficiently dense [16] and always needed to be post-treated, e.g., by hot isostatic pressing (HIP). Process optimization alone is laborious, although promising for single-step fabricating ceramics by SLM and LDED processes. The process window for high-quality LDEDed ceramics was narrow due to higher thermal stress and crack susceptibility [61]. In addition, the voids and cracking of LDEDed Al_2O_3 parts were significantly reduced when the substrate material was changed from Al_2O_3 to Ti-6Al-4V alloy [59]. Preheating powder bed or substrate for LAM effectively decreases thermal stress to reduce cracking. The main energy sources for preheating are laser beams [23, 70], induction heating [73], and microwaves [74]. However, the poor surface quality of preheated parts is a tricky issue, such as the significant increase in R_a of SLMed ceramics (**Fig. 3(e)**) [75]. The cost and safety are other issues that need to be noted. For an ultrasound-assisted deposition condition, mechanical, cavitation, and acoustic flow effects created by ultrasonic vibrations can promote rapid fluid flow on both sides of the melt pool, significantly reducing porosity and decreasing the possibility of cracking [72, 76]. The addition of enhancement phases to fabricate LAMed composite ceramics creates a variety of toughening mechanisms, and increasing the energy required for crack formation and propagation can also inhibit defect formation. Mechanical agitation of the hard particles or fiber during the LAM process also provides the potential for bubble breakage and escape. These reinforcing phases are mainly ZrO_2 [38], SiC [77], and C_f [78]. Furthermore, regranulation [79], laser remelting [80], and scanning strategy optimization [59] are other effective approaches to suppress defects in LAMed ceramics. This is because these approaches modulate the thermal history and the mass-energy transport in the melt pool. Therefore, the in-depth revelation of thermal mass flow in the melt pool is a prerequisite for further understanding the voids formation mechanism.

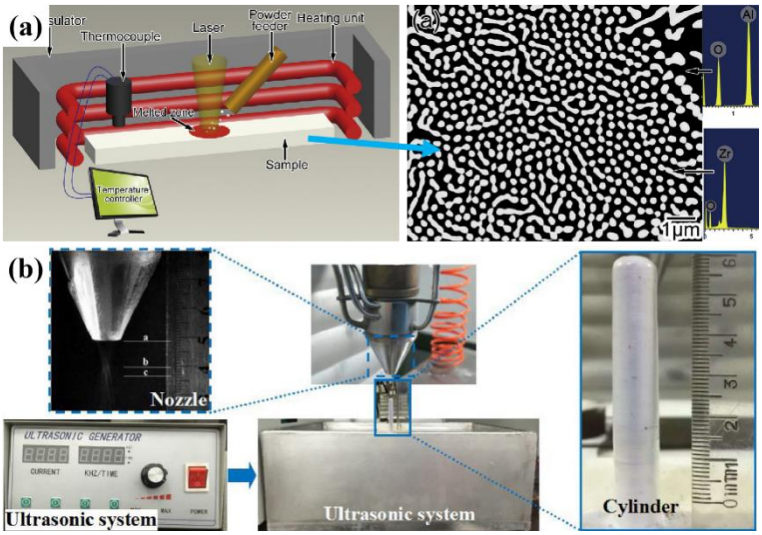

Fig. 8 Defect inhibition approaches in LAM-processed ceramics: (a) preheating [73], (b) ultrasound assistance [36].

4 Microstructures of directly LAMed ceramics

Directly LAMed ceramics have a microstructure different from conventional sintering due to particular process principles and complex thermal histories, and these key features influence the part performance. This section focuses on Al_2O_3 and Al_2O_3-based composites, interspersed with other single-phase ceramics, and discusses the microstructure of directly LAMed ceramics.

4.1 Al_2O_3 ceramics

The microstructure of Al_2O_3 ceramics fabricated by SLS/SLM with solid sintering or partial melting is partially dense, consisting of a near powder-like structure and consolidated Al_2O_3 droplets separated by pores [64], as shown in **Fig. 9(a-b).** The spherical structure size (grain size) of the consolidated Al_2O_3 can be controlled by optimizing process parameters [12]. While the microstructure of a single track Al_2O_3 ceramics produced by SLS/SLM with full melting is dominated by columnar dendrites. Equiaxial dendrites are formed at the top of the single passes when the Q is increased to a certain level (**Fig. 9(c)**). Fully melting of Al_2O_3 ceramics using laser seems difficult due to the reflection and low absorption rate of laser radiation. The microstructure can be optimized to promote anisotropic grain growth or equiaxialization by doping micro-metal oxide to increase the absorption rate and improve the powder bed density [81]. The LDEDed Al_2O_3 grains tend to grow epitaxially in the build direction. In contrast, the other directions are suppressed due to the strong one-dimensional heat loss of the solidification layer through the substrate, regularly arranged in parallel [28]. The textured Al_2O_3 ceramics maintain a single-phase composition consistent with the initial

material, which is stable α-Al_2O_3 [29]. Increasing the *v* inhibits grain growth and triggers the transition from columnar to equiaxed crystals, resulting in grain refinement [82]. Furthermore, optimizing the scanning strategy also seems to optimize the microstructure [59], similar to the process parameters by controlling the solidification conditions (*G* and *R*), but further investigation is needed.

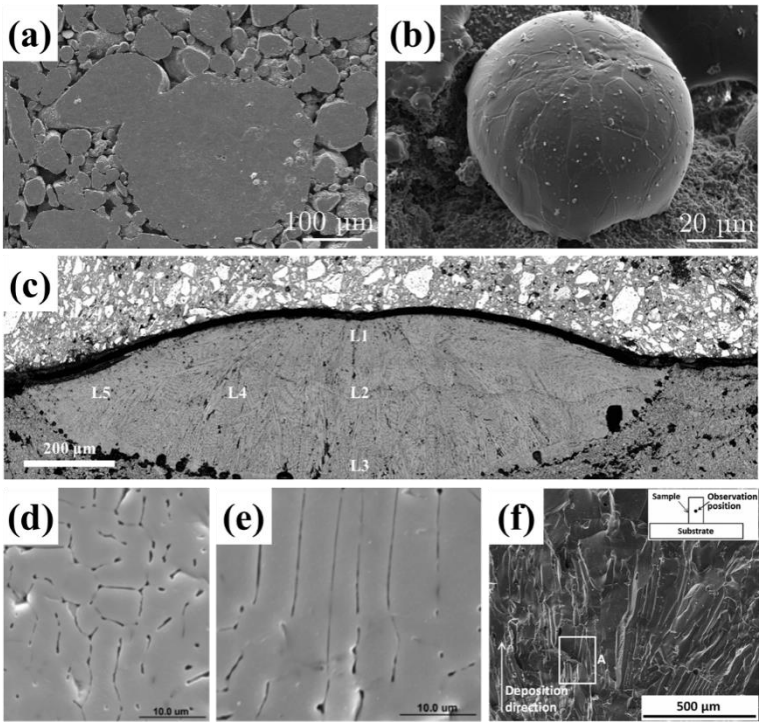

Fig. 9 Microstructure characteristics of Al_2O_3 ceramics fabricated by LAM processes: (a) and (b) SLS/SLM [64], (c) SLM [13], (d), (e), and (f) LDED [28, 29].

4.2 Al_2O_3-based composites

Oxide eutectic ceramics, also known as melt growth composites (MGC), prepared by directional solidification, have stirred great enthusiasm in the field of LAM ceramics due to their excellent properties [83]. The typical microstructure of the LAMed Al_2O_3/ZrO_2 eutectic ceramics is a structure consisting of light *t*-ZrO_2 embedded in a dark α-Al_2O_3 matrix [23], as shown in **Fig. 10(a)**. Specifically, fine and regular lamellar *t*-ZrO_2 are diffused in the columnar Al_2O_3 colony structure. These two phases are in nanoscale and the phase interface is clean and free of amorphous phases [33], with a eutectic spacing of about 50-100 nm (**Fig. 10(b)**). Moreover, in LAMed eutectic ceramics, periodic banded structures (PBSs) along the build direction are a noteworthy feature because they significantly affect mechanical properties (**Fig. 10(c-d)**) [41, 80, 84]. The thermal influence of the upper deposited layer, the epitaxial growth of the solidified microstructure, and the microstructural coarsening behavior (MCZs), similar

to that of the heat-affected zone (HAZ) in laser welding have been applied to explain the formation of PBSs in LAMed eutectic ceramics. However, the relationship between PBSs and the deposited layers interface needs to be revealed. For example, EBSD analysis at the boundary of PBSs containing coupled zone, transition zone, and HAZ, reveals a random crystallographic orientation attributed to the initial uncoupled growth at the bottom of a melt pool (**Fig. 10(e)**) [35]. This provides detailed information about the relationship between PBSs and deposited layers. In contrast, in rapid directional solidification, the formation of PBSs can be intuitively explained as periodic oscillations of the solidification interface [85]. Therefore, the formation mechanism of PBSs found in LAMed eutectic ceramics seems to require a more detailed investigation. It is worth pointing out that the microstructure of LAMed Al_2O_3/ZrO_2 composites can be optimized after adjusting material composition, showing the evolution patterns of microstructure with cellular, undeveloped dendritic, dendritic for hypoeutectic ceramics, or the opposite for hypereutectic ceramics. In addition, three-dimensional quasi-continuous network structures (3DQCN) have also been found in LAMed composites when ZrO_2 is below the eutectic ratio, which is believed to contribute to mechanical property enhancement [34].

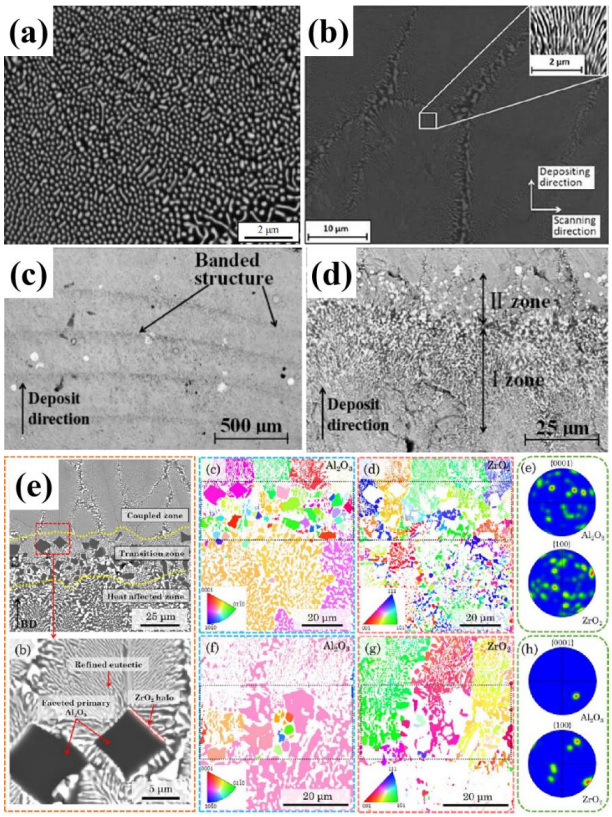

Fig. 10 Microstructure characteristics of Al_2O_3/ZrO_2 eutectic and composites fabricated by LAM processes: (a) SLMed Al_2O_3/ZrO_2 eutectics [23], (b) LDEDed Al_2O_3/ZrO_2 composites [86], (c), (d), and (e) LDEDed Al_2O_3/ZrO_2 eutectics [35, 84].

$Al_2O_3/Y_3Al_5O_{12}$ (YAG) and $Al_2O_3/GdAlO_3$ (GAP) eutectic are another two cases of binary eutectic ceramics fabricated by LAM processes. The dominant microstructure of LDEDed Al_2O_3/YAG eutectic ceramics is the three-dimensional interpenetrating network structure ('Chinese script' patterns) with fine irregular eutectic, comprising of a dark Al_2O_3 phase and a bright YAG phase, shown in **Fig. 11.** The formation of irregular eutectic is related to the higher melting entropy of the two phases. In this case, the Al_2O_3 grows continuously along the $\langle 10\bar{1}0 \rangle$ crystallographic orientation, while the YAG changes from random to competitive growth, which can be explained by the Magnin-Kurz model [42]. Substrate water cooling can change the microstructure from a typical network structure to a colony and dendritic structure, and the eutectic spacing will be reduced by 78.1% [87]. Correspondingly, the HAZ roughly affected the microstructure of SLS/SLMed Al_2O_3/GAP eutectic ceramics between adjacent deposited layers, in which the Al_2O_3 and GAP phases were uniform 'Chinese script' patterns [26]. The microstructure inside the deposited layers is typical of a colony structure, consisting of 'Chinese script' patterns, lamellar patterns, and rod-like patterns.

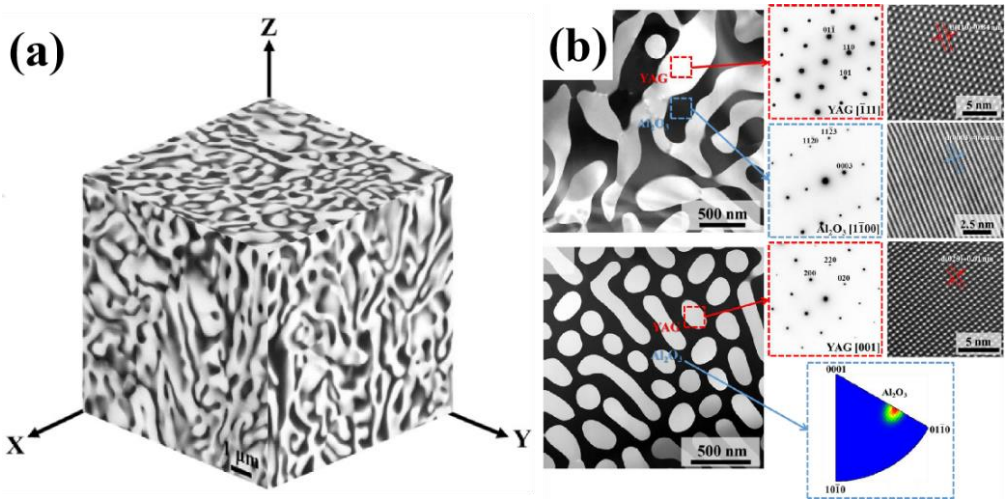

Fig. 11 Interfacial structures of Al_2O_3/YAG eutectic ceramics fabricated by LDED process [42].

One of the cases for ternary eutectic ceramics fabricated by LAM is $Al_2O_3/GdAlO_3/ZrO_2$. The key feature of the microstructure for SLS/SLMed $Al_2O_3/GdAlO_3/ZrO_2$ is the colony structure with a 'Chinese script' patterns, lamellar patterns, and rod-like patterns, internally composed of a black Al_2O_3 phase, a gray ZrO_2

phase, and a white $GdAlO_3$ phase [27]. Similarly, the microstructure of LDEDed $Al_2O_3/GdAlO_3/ZrO_2$ ternary eutectic ceramics also has eutectic structures such as colony structure and 'Chinese script' patterns, shown in **Fig. 12.** Moreover, another ternary eutectic ceramics fabricated by LDED is $Al_2O_3/YAG/ZrO_2$ [41], with the microstructure of monocrystal cellular eutectics. The texture along the building direction is $<0001>_{Al2O3}//<001>_{YAG}//<001>_{ZrO2}$, gradually inclined from the center to the edge.

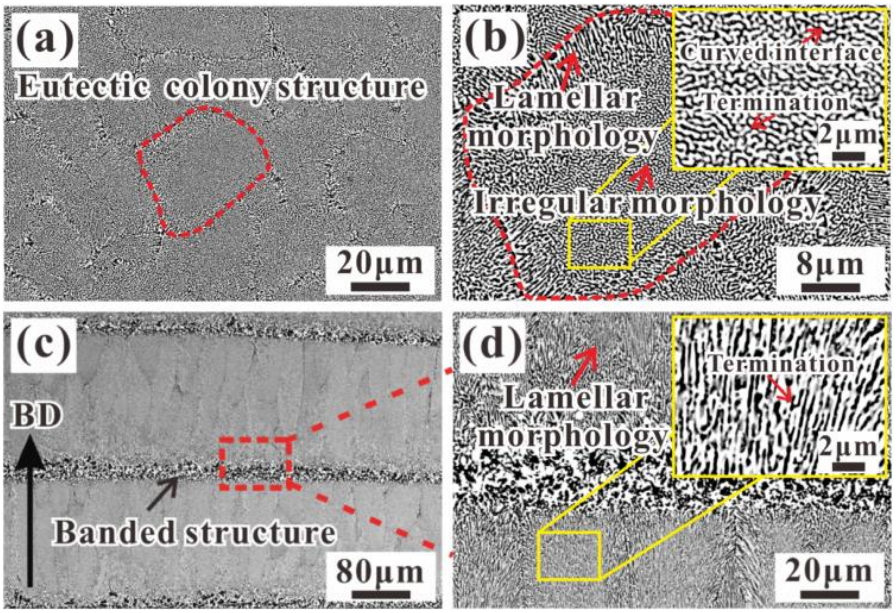

Fig. 12 Microstructure characteristics of $Al_2O_3/GdAlO_3/ZrO_2$ ternary eutectic ceramics fabricated by LDED process [88].

In situ synthesized Al_2O_3/Al_2TiO_5 [89] and Al_2O_3/mullite [43] are other representatives of LAMed Al_2O_3-based composites. They usually contain in situ synthesized Al_2TiO_5 or mullite dispersed in the continuous Al_2O_3 matrix (**Fig. 13**) [39]. The morphology and content of the Al_2TiO_5 phase or mullite phase vary with process parameters and material composition under the influence of solidification conditions (*G* and *R*). For example, with increasing *Q*, the microstructure of LDEDed Al_2O_3/Al_2TiO_5 composites deposited by Al_2O_3 and TiO_2 powders evolves from isotropic growth to anisotropic growth, which the non-equilibrium solidification theory can explain. Similarly, as the Al_2O_3 content in the initial material increases, the microstructure of LDEDed Al_2O_3/mullite composites deposited by Al_2O_3 and SiO_2 powders evolves from anisotropic growth (equiaxial dendrites) to isotropic growth (columnar crystals), which can be explained by the nucleation theory and compositional supercooling theory.

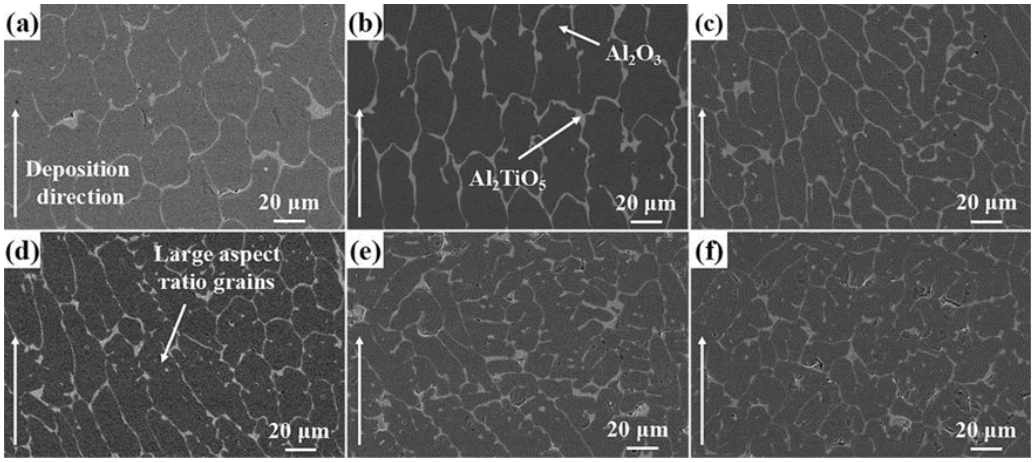

Fig. 13 Microstructure characteristics of Al_2O_3/Al_2TiO_5 composites fabricated by LDED process [49].

4.3 Other ceramics

In the case of SLS/SLMed SiO_2 ceramics, the sand particles were sintered together but underwent partial melting due to the low energy input. Additionally, the surfaces of particles were melted and connected through 'bridges' [54]. The microstructure of SLS/SLMed Y_2O_3 stabilized ZrO_2 (YSZ) is columnar structures aligned along the build direction with elongated shape grains resulting from the blend of graphite and YSZ, as shown in **Fig. 14**. In another case, bonding was observed between the powder particles, and only surface melting and bonding occurred between the particles, with no apparent grain boundaries [15]. The SLS/SLMed Y_2O_3 ceramics also exhibit partial melting features with particle agglomeration, and the agglomerated particles are further sintered after the heat treatment under vacuum at a high temperature [20]. Particle clusters and needle-like protrusions parallel to the scanning direction are another feature of SLS/SLM SiC ceramics when the powder binding mechanism is partially melting or not melting [90]. Furthermore, the microstructure of SLS/SLMed $BaTiO_3$ ceramics shows longer large grains with an average grain of 120 μm and a secondary phase along the grain boundaries [21]. Other representatives of ceramics produced using the LDED processes are $MgAl_2O_4$ and mullite. LDEDed $MgAl_2O_4$ ceramics consist of the dark spinel phase ($MgAl_2O_4$) and the light secondary phase ($MgO{\cdot}1.4Al_2O_3$) [31]. The average grain size of $MgAl_2O_4$ gradually increases with increasing *P*. Another attractive ceramic is mullite, synthesized using high-purity Al_2O_3 and SiO_2 powders [51]. The microstructure of the LDEDed cylindrical mullite samples is characterized by central 'tabular cellular' and marginal 'rod cellular', as shown in **Fig. 14(c)**, with an over-evolution from the center to the edges, which is determined by the difference in heat

dissipation at different locations in the melt pool. The process parameters have an essential influence on the crystal structure of mullite [32].

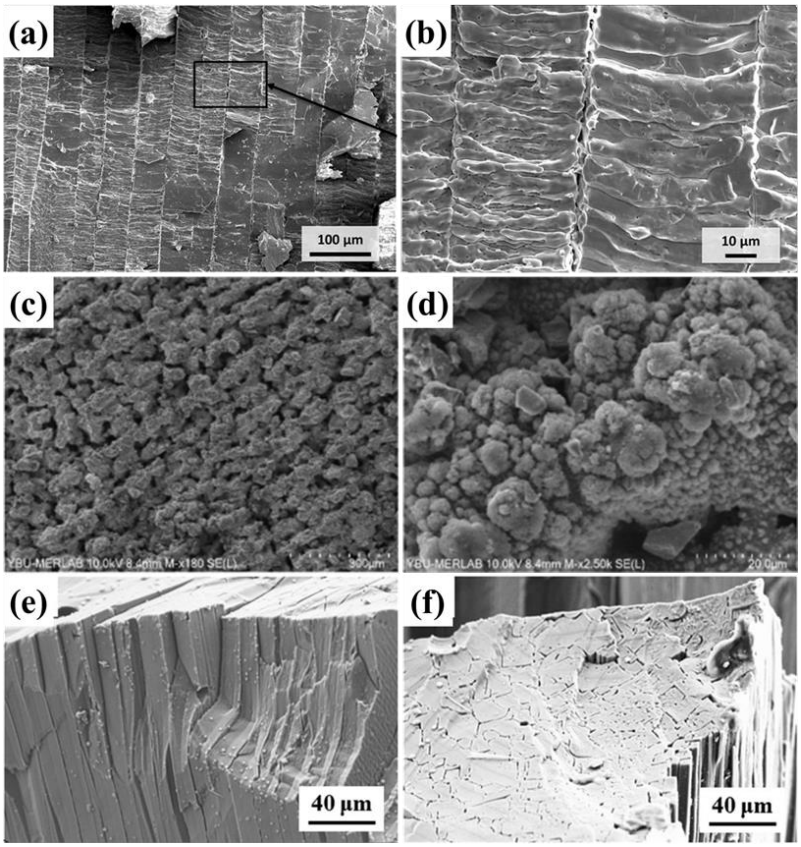

Fig. 14 Microstructure characteristics of ZrO_2, mullite, and SiC fabricated by LAM processes: (a) and (b) direct SLSed ZrO_2 [15], (c) and (d) direct SLSed SiC [17], (e) and (f) LDEDed mullite [51].

5 Mechanical properties of direct LAM ceramics

In this section, the mechanical properties of ceramics fabricated by the LAM processes are recapitulated, with particular emphasis on relationships between process parameters, defects, microstructure, and properties, as well as the influence of external field assistance and post-treatment. The mechanical properties and enhancement methods of LAMed ceramics are summarized in **Tables 5 and 6**, respectively.

5.1 Fracture toughness and microhardness

A key parameter associated with the serviceability and quality of ceramics is the fracture toughness (K_c), which refers to their ability to resist crack propagation. Given the presence of defects such as microcracks and pores in LAMed ceramics with brittle and hard characteristics, evaluating and enhancing K_c is crucial for achieving high-quality ceramics through LAM. The K_c of LAMed ceramics has been investigated on various ceramic materials, as listed in **Table 5**. Generally, the K_c of LAMed ceramics

is comparable to or lower than that of conventionally sintered ceramics due to high-energy laser processing and strong crack sensitivity. The K_c is related to the intrinsic properties, microstructure, and defects of ceramics. Firstly, as described in previous sections, material compositing is one of the effective ways to tailor the microstructure directly, which can limit crack tip formation and further propagation. A typical representative is zirconia toughened alumina (ZTA) ceramics. LAMed ZTA ceramics can exhibit excellent K_c when changing material composition [34, 37, 91]. Notably, when the composition is a eutectic ratio, the nanoscale eutectic spacing significantly limits the crack propagation [75, 92]. Moreover, the stress-induced volume increase caused by the ZrO_2 phase transition (t-ZrO_2 to m-ZrO_2) is also a key factor for the increase in toughness in this material system. When the grain morphology of high-modulus strengthening phases (ZrO_2 [91], Al_2O_3 [43, 49], and SiC [77]) changes from columnar crystals or columnar colonies to dendrites, the energy required for crack expansion increases, triggering the formation of toughening mechanisms such as crack deflection, branching, pinning, bridging, and microcracks. Secondly, by manipulating the thermal history of the LAM processes [39], process optimization affects the solidification parameters (G and v_s), which ultimately results in microstructure modulation to limit crack tip formation and further propagation. However, deposited parts are prone to cracking when the process parameters used exceed the threshold of LED, while using too low LED tends to form a melt pool with poor quality. Finally, as a method to affect thermal history and adjust microstructure, external field assistance is also a way to improve the properties of LAMed ceramics, such as ultrasound-assistance [76, 92] and water-cooling [87], as listed in **Table 6.** Due to the cavitation perturbation and mechanical stirring effects, a uniform and fine microstructure (nanoscale) of LAMed ceramics assisted by ultrasound [73] is beneficial for increasing K_c. Correspondingly, water-cooling of the substrate weakens the heat accumulation and significantly increases the cooling rate [87]. The microstructure of LAMed ceramics transforms from a typical 3D network structure to a colony and dendrite structure with grain refinement, increasing K_c.

Because of its convenience, the indentation method is often used to measure the Vickers microhardness (H_v) of LAMed ceramics. The key elements that determine microhardness are crystal structure, density, grain orientation (e.g., texture), and grain size. The crystal structure depends on the atomic bonding of materials. Different ceramics exhibited different levels of microhardness values (**Table 5**). Density is one

of the most critical factors affecting the microhardness of SLS/SLMed ceramics with solid sintering or partial melting. Increasing energy density and compacting powder bed contribute to densification, increasing microhardness. Because the microstructure of LAMed ceramics with full melting tends to grow epitaxially along the build direction, forming the columnar crystals, the microhardness tends to exhibit anisotropy with higher microhardness in the build direction than the scanning direction [41, 43]. According to the Hall-Petch relationship, ceramics with small grain sizes possess high microhardness. Accordingly, controlling the process parameters, applying external fields to increase the G or R to reduce the grain size, and adding high-modulus reinforcing phases increase the microhardness of LAMed ceramics. For example, low Q leads to grain refinement and, as a result, increases the microhardness of SLS/SLMed Al_2O_3 ceramics [13]. After ultrasound assistance, LDEDed Al_2O_3/ZrO_2 ceramics showed a significant increase in microhardness and wear resistance due to grain refinement [76].

Table 5 Mechanical properties of ceramics fabricated by the LAM processes

Author	Materials	Processes	P (W)	v (mm/min)	σ_{fs} (MPa)	K_c (MPa·m$^{1/2}$)	H_v (GPa)
Fayed [12]	Al_2O_3	SLS/SLM	230	150	N/A	N/A	16.5 ± 1.1
Fan [13]	Al_2O_3	SLS/SLM	100-400	300-1000	N/A	N/A	16.3-18.3
Balla [28]	Al_2O_3	LDED	175	600	N/A	2.1 ± 1.3	15.2 ± 0.9
Niu [61]	Al_2O_3	LDED	375	300	210, 350 (max)	N/A	N/A
Liu [14]	ZrO_2	SLS/SLM	30-90	0.6-12	N/A	N/A	11.4 ± 2.6
Fan [30]	ZrO_2	LDED	250-350	355	N/A	N/A	19.1-19.8
Wilkes [75]	Al_2O_3/ZrO_2	SLS/SLM	48-60	1200	173.8-538.1	6.2-9.1	14.9-15.4
Yves-Christian [63]	Al_2O_3/ZrO_2	SLS/SLM	60	1200	>500	N/A	N/A
Niu [33]	Al_2O_3/ZrO_2	LDED	410	400	N/A	4.79	16.8
Ma [71]	Al_2O_3/ZrO_2	LDED	530	400	N/A	3.71 ± 0.3, 4.79 ± 0.3	17.15 ± 0.4
Yan [84]	Al_2O_3/ZrO_2	LDED	300-450	300-450	N/A	6.52	18.59
Li [37]	Al_2O_3/ZrO_2	LDED	N/A	200	N/A	3.24-5.76	17.5-21.4
Hu [34]	Al_2O_3/ZrO_2	LDED	350	600	N/A	2.63-3.64	14.4-18.5
Pappas [38]	Al_2O_3/ZrO_2	LDED	275	1000	103, 208	3.4, 3.8	16.5, 17.7
Shen [26]	$Al_2O_3/GdAlO_3$	SLS/SLM	100-450	4-60	N/A	4.5 ± 0.1	17.1 ± 0.2
Wu [89]	Al_2O_3/Al_2TiO_5	LDED	250	400	~200-270	1.10-3.97	>1670
Huang [49]	Al_2O_3/Al_2TiO_5	LDED	250	50-900	~47.5-212	2.9-3.75	14.7-16.7

Huang [39]	Al_2O_3/Al_2TiO_5	LDED	150-350	300	142.59-227.41	3-3.87	13.7-15.7
Zhao [43]	Al_2O_3/mullite	LDED	300	250	310.1 ± 36.5	CS: 2.00 ± 0.18-3.07 ± 0.13 LS: 1.95 ± 0.24-3.01 ± 0.18	CS: 14.54 ± 18.39 ± 0.38 LS: 13.99 ± 0.11
Fan [41]	$Al_2O_3/YAG/ZrO_2$	LDED	220	558	N/A	CS: 3.53 ± 0.32 LS: 3.84 ± 0.44	CS: 20.6 ± 0.6 LS: 20.5 ± 0.6
Liu [27]	$Al_2O_3/GdAlO_3/ZrO_2$	SLS/SLM	200	6	N/A	6.1-7.8	14.3-15.3

* CS = Cross section, LS = Longitudinal section.

Table 6 Mechanical properties of ceramic materials fabricated by LAM processes under external field assistance and post-treatment

Author	Materials	Processes	Improvement of processes	σ_{fs} (MPa), Max#	K_c (MPa·m$^{1/2}$), Max#	H_v (GPa), Max#
Balla [28]	Al_2O_3	LDED	Heat treatment, 1000 ℃/5 h Heat treatment, 1600 ℃/5 h	N/A	4.4 ± 1.4, 109.52%	16.66 ± 0.35, 9.25%
Zhao [93]	Al_2O_3	LDED	Heat treatment, 500-1600 ℃	378.59-494.15, 83%	2.71-2.94, 3.16%	18.26-18.69
			Heat treatment, 5-20 h	471.04-547.85, 102.96%	2.84-3.07, 7.72%	18.38-19.19
Zhao [94]	Al_2O_3+ trace SiO_2	LDED	Heat treatment, 1000-1400 ℃/4 h	382.92-504.38, 62.65%	3.09-3.54, 16.83%	18.16-18.64, 2.47%
Verga[95]	Al_2O_3+TiC	SLS/SLM	Heat treatment, 900 ℃/3 h	181, 232 (max)	N/A	N/A
Liu [60]	$Al_2O_3/GdAlO_3/ZrO_2$	LDED	Heat treatment, 1300-1500 ℃/200 h	N/A	3.69-4.04, 9.49%	15.5-13.01, -17.87%
Liu [96]	$Al_2O_3/GdAlO_3/ZrO_2$	LDED	Heat treatment, 1200 ℃/1-8 h	N/A	3.40 ± 0.36, -3.9%	15.79 ± 0.44, 12.96%

Yan [92]	Al_2O_3/ZrO_2	LDED	Ultrasound-assisted, 20-160 W	N/A	7.67 ± 0.2, 17.64%	16.22
Yan [78]	Al_2O_3/ZrO_2+C_f	LDED	Ultrasound-assisted, 120 W	N/A	8.7 ± 0.2, 33.44%	N/A
Hu [76]	Al_2O_3/ZrO_2	LDED	Ultrasound-assisted, 41 kHz, 5 μm*	N/A	N/A	17.15, 5.28%
Wu [87]	$Al_2O_3/Y_3Al_5O_{12}$	LDED	Water cooling assisted, 28 ℃	N/A	5.86 ± 1.11, 8.5%	21.5 ± 2.7, 10.6%

* Ultrasound frequency = 41 kHz, Ultrasound amplitude =5 μm.

Maximum change compared to as-fabricated (%).

5.2 Flexural strength

One of the prerequisites for using ceramic materials is that their flexural strength (σ_{fs}) meets engineering requirements, especially when used as high-temperature structural material. Generally, the flexural strength of LAMed ceramics can reach the same order of magnitude as conventional sintering. For instance, a maximum value of 538.1 MPa for SLS/SLMed Al_2O_3/ZrO_2 composites [75], and 350 MPa for LDEDed Al_2O_3 ceramics [29]. However, the dispersion of strength values is relatively wide, which is related to the brittle fracture and the inhomogeneity defects of LAMed ceramics. For example, the average flexural strength value of LDEDed Al_2O_3 is only 210 MPa [29], and that of the SLS/SLMed Al_2O_3/ZrO_2 composites is 208 MPa [38]. Hence, strength dispersion is an issue for LAMed ceramics. Further, according to the Hall-Petch relationship and the empirical relationship of strength/porosity [43], porosity and grain size seem to be two vital factors affecting the σ_{fs} of LAMed ceramic materials, and their relationship with strength is negatively correlated. The porosity of LDEDed Al_2O_3/ZrO_2 composites decreases significantly when the Q increases, while the grain size may increase gradually [91]. Accordingly, Huang [39] believes that the σ_{fs} usually shows a parabolic law that increases first and then decreases. The effect of microscopic defects on σ_{fs} seems not negligible considering the strength dispersion. The study [43] for LAMed Al_2O_3/mullite composites also found that the σ_{fs} of Al_2O_3 ceramics was significantly enhanced (up to 310 MPa on average) with the addition of a small amount of SiO_2 (3 wt%), and the strengthening appeared to be due to the reduction of defects and residual stress, increase in the modulus, and change in the fracture pattern. However, the strength properties are still insufficient. Subsequent heat treatment of the LAMed parts may be a viable solution to further enhance the mechanical properties of LAMed ceramics [93-95] due to residual stress relief, crack healing, and possibly grain size reduction.

6 Summary and outlook

Powder-based direct LAM processes, which encompass powder beds and powder feeding, have sparked considerable excitement across various industries such as aerospace and energy. This excitement stems from their potential to manufacture ceramic parts with dense and intricate shapes in a single step. However, the development of direct LAM for ceramics has been slower compared to metals and polymers. The fabrication of LAM ceramics faces significant scientific and technological challenges, including the meticulous regulation and control of quality,

defects, microstructures, and properties of LAMed ceramic parts. One major obstacle to the direct LAM of high-performance ceramics, particularly concerning geometric and mechanical properties, is the inherent brittleness and low thermal shock tolerance juxtaposed with the need to withstand extremely high temperatures and repetitive thermal cycling. Recent publications on LAM-processed high-quality ceramics offer insights into potential trends in addressing these challenges.

(1) High-fidelity and high-efficiency numerical simulation and data-driven approach to support process optimization.

There remains a significant gap between the geometric properties of LAMed ceramics and the actual requirements of various industries. Hence, optimizing different processing parameters becomes crucial for directly manufacturing high-performance ceramic parts, even though the process window for fabricating crack-free parts appears to be narrow. Numerical simulations of critical physical fields of the LAM processes, such as temperature/stress and thermofluidic transport properties, may offer a viable solution for optimizing parameters and investigating process features of LAMed ceramics. Build strategies based on a data-driven approach, such as machine learning, enables the direct optimization of process parameters based on part performance and enhances simulation efficiency. However, this approach necessitates the collection and analysis of substantial amounts of high-quality process data. Moreover, the challenge posed by extremely high process temperatures for data collection needs to be addressed. The development and application of online and real-time detection technologies show promise in overcoming this challenge.

(2) New crack initiation/propagation theory and inhibition strategy.

Cracking is the primary restriction for direct LAM of ceramic parts with large sectional dimensions. Preheating to assist the LAM processes, such as LAMed Al_2O_3/ZrO_2, is deemed advantageous for addressing this issue. Nonetheless, the effect of preheating, whether it pertains to the substrate or the ambient environment during the deposition process, on the metallurgical state of powder particles in the shaping process seems complicated to ignore. For instance, preheating can lead to worsened surface roughness of ceramic parts fabricated via the powder bed process. Introducing ultrasonic vibration can mitigate the tendency for cracking by enhancing the solidification environment of the melt pool and alleviating thermal stress through the uniform dispersion of materials. Nevertheless, the crack suppression effect appears to

be limited and the surface roughness of the LAMed ceramic parts is poor. Directly observing fracture damage in brittle materials, particularly microcracking induced by thermal stress, is challenging. However, the speed of crack propagation seems to be influenced by the extent of material stretching at the crack tip front [97]. Therefore, inducing compressive stress at the crack front, such as through martensite phase transformation, timely material replenishment at the crack front [98], and filling crevasses, may offer effective solutions for inhibiting cracking in LAMed ceramics.

(3) New theory and approach for voids formation and control.

Several investigations have demonstrated the feasibility of the LAM processes in achieving ceramics with density close to 100%. However, achieving complete void elimination appears to be unattainable, particularly for materials with viscous properties like Si-based ceramics [19]. While analyzing gas solubility reduction and bubble movement in the melt pool can help understand the mechanism of pore formation. The unique metallurgical conditions involved in LAM processes, such as high cooling rates, repetitive thermal cycling, and heat accumulation, contribute to a significantly complex pore formation mechanism compared to traditional processes like casting and welding. Therefore, further experimental observations and theoretical analyses of the physical processes are crucial to reducing the tendency for cracking caused by stress concentration. The development of online or offline observation methods for voids is expected to significantly advance our understanding of this issue.

(4) New approaches to the control of microstructure and properties.

The distinctive heat dissipation characteristic of LAMed ceramics often leads to a textured grain arrangement, such as epitaxial growth along the build direction, thereby resulting in anisotropic properties. The rapid solidification process, which causes an inhomogeneous microstructure distribution, leads to varying properties across different locations of the parts. Implementing field-assisted techniques, such as ultrasound or magnetic fields, to drive grain equiaxialization and nanosizing, can be potential solutions to counter thermally driven forces and the high entropy melting of ceramics. These approaches have the potential to significantly enhance the mechanical properties of LAMed ceramics.

(5) Development of new processes for direct LAM processes ceramic powders.

The raw powder currently used is primarily tailored for traditional industries on a large scale. However, given the unique process features of LAM, developing

specialized powders could serve as an alternative approach to manufacturing high-performance ceramics in a single step. This could involve designing and enhancing materials at the source, such as through re-granulation or surface modification of the raw ceramic powder.

(6) Possible applications for LAMed ceramics.

LAMed ceramics offer potential applications in specific small-sized bulk parts, such as precision cutting tools in mechanical manufacturing, automotive seal rings and brakes, hip prostheses for musculoskeletal hard connective tissues in dental, precision pinions for smart factories, and ceramic thermometry sensors that require subsequent processing. Additionally, the preparation of high-quality ceramic coatings presents an interesting application avenue. For instance, ceramic coatings produced using ultra-high-speed LAM are expected to significantly enhance wear and corrosion resistance by reducing cracking. However, there remains a significant disparity between the pressing demand for large-sized and complex-shaped parts across various industries and the current capabilities of direct LAM processes in fabricating high-performance ceramics. This indicates that more efforts will be necessary to overcome these scientific and technical challenges in the future.

Acknowledgments

The authors are grateful for the sponsorship of the following fund projects: the Guangzhou Basic and Applied Basic Research Project (No. 2024A04J00725), the GDAS' Project of Science and Technology Development (No. 2022GDASZH-2022010107, No. 2022GDASZH-2022010108).

Reference

[1] N. P. Padture, Advanced structural ceramics in aerospace propulsion, *Nat. Mater.*, 15(2016), No.8, p. 804.

[2] S. J. Zinkle and G. S. Was, Materials challenges in nuclear energy, *Acta Mater.*, 61(2013), No.3, p. 735.

[3] C. L. Cramer, E. Ionescu, M. Graczyk-Zajac, A. T. Nelson, Y. Katoh, J. J. Haslam, L. Wondraczek, T. G. Aguirre, S. LeBlanc, H. Wang, M. Masoudi, E. Tegeler, R. Riedel, P. Colombo and M. Minary-Jolandan, Additive manufacturing of ceramic

materials for energy applications: road map and opportunities, *J. Eur. Ceram. Soc.*, 42(2022), No.7, p. 3049.
[4] K. P. Misra and R. D. K. Misra, Advanced ceramics, *Ceram. Sci. Engin.*, (2022), 21-43.
[5] M. Schmidt, M. Merklein, D. Bourell, D. Dimitrov, T. Hausotte, K. Wegener, L. Overmeyer, F. Vollertsen and G. N. Levy, Laser based additive manufacturing in industry and academia, *CIRP Ann-Manuf. Technol.*, 66(2017), No.2, p. 561.
[6] S. Dadhania, 3D Printing Ceramics 2022-2032: Technology and Market Outlook, (2022).
[7] J. P. Kruth, G. Levy, F. Klocke and T. H. C. Childs, Consolidation phenomena in laser and powder-bed based layered manufacturing, *CIRP Ann-Manuf. Technol.*, 56(2007), No.2, p. 730.
[8] M. Dadkhah, J.-M. Tulliani, A. Saboori and L. Iuliano, Additive manufacturing of ceramics: advances, challenges, and outlook, *J. Eur. Ceram. Soc.*, 43(2023), No.15, p. 6635.
[9] S. Pfeiffer, K. Florio, D. Puccio, M. Grasso, B. M. Colosimo, C. G. Aneziris, K. Wegener and T. Graule, Direct laser additive manufacturing of high performance oxide ceramics: a state-of-the-art review, *J. Eur. Ceram. Soc.*, 41(2021), No.13, p. 6087.
[10] Y. Lakhdar, C. Tuck, J. Binner, A. Terry and R. Goodridge, Additive manufacturing of advanced ceramic materials, *Prog. Mater. Sci.*, 116(2021), p. 100736.
[11] E. Juste, F. Petit, V. Lardot and F. Cambier, Shaping of ceramic parts by selective laser melting of powder bed, *J. Mater. Res.*, 29(2014), No.17, p. 2086.
[12] E. M. Fayed, A. S. Elmesalamy, M. Sobih and Y. Elshaer, Characterization of direct selective laser sintering of alumina, *Int. J. Adv. Manuf. Technol.*, 94(2017), No.5-8, p. 2333.
[13] Z. Fan, M. Lu and H. Huang, Selective laser melting of alumina: a single track study, *Ceram. Int.*, 44(2018), No.8, p. 9484.
[14] Q. Liu, B. Song and H. Liao, Microstructure study on selective laser melting yttria stabilized zirconia ceramic with near IR fiber laser, *Rapid Prototyping J.*, 20(2014), No.5, p. 346.
[15] L. Ferrage, G. Bertrand and P. Lenormand, Dense yttria-stabilized zirconia obtained by direct selective laser sintering, *Addit. Manuf.*, 21(2018), p. 472.
[16] P. Bertrand, F. Bayle, C. Combe, P. Goeuriot and I. Smurov, Ceramic components manufacturing by selective laser sintering, *Appl. Surf. Sci.*, 254(2007), No.4, p. 989.

[17] M. Abdelmoula, G. Küçüktürk, D. Grossin, A. M. Zarazaga, F. Maury and M. Ferrato, Direct selective laser sintering of silicon carbide: realizing the full potential through process parameter optimization, *Ceram. Int.*, 49(2023), No.20, p. 32426.

[18] M. X. Gan and C. H. Wong, Properties of selective laser melted spodumene glass-ceramic, *J. Eur. Ceram. Soc.*, 37(2017), No.13, p. 4147.

[19] K. C. Datsiou, E. Saleh, F. Spirrett, R. Goodridge, I. Ashcroft and D. Eustice, Additive manufacturing of glass with laser powder bed fusion, *J. Am. Ceram. Soc.*, 102(2019), No.8, p. 4410.

[20] A. Ratsimba, A. Zerrouki, N. Tessier-Doyen, B. Nait-Ali, D. André, P. Duport, A. Neveu, N. Tripathi, F. Francqui and G. Delaizir, Densification behaviour and three-dimensional printing of Y_2O_3 ceramic powder by selective laser sintering, *Ceram. Int.*, 47(2021), No.6, p. 7465.

[21] X. Zhang, F. Wang, Z. Wu, Y. Lu, X. Yan, M. Nastasi, Y. Chen, Y. Hao, X. Hong and B. Cui, Direct selective laser sintering of hexagonal barium titanate ceramics, *J. Am. Ceram. Soc.*, 104(2020), No.3, p. 1271.

[22] X. Zhang, N. Li, X. Chen, M. Stroup, Y. Lu and B. Cui, Direct selective laser sintering of high-entropy carbide ceramics, *J. Mater. Res.*, 38(2022), No.1, p. 187.

[23] J. Wilkes, Y. C. Hagedorn, W. Meiners and K. Wissenbach, Additive manufacturing of ZrO_2-Al_2O_3 ceramic components by selective laser melting, *Rapid Prototyping J.*, 19(2013), No.1, p. 51.

[24] F. Verga, M. Borlaf, L. Conti, K. Florio, M. Vetterli, T. Graule, M. Schmid and K. Wegener, Laser-based powder bed fusion of alumina toughened zirconia, *Addit. Manuf.*, 31(2020), p. 100959.

[25] Y. Zhang, K. Zhang, D. Chen, T. Liu, Z. Xiong, S. Li, F. Li and Z. Zhu, Morphology and formation mechanism of cracks in Al_2O_3–ZrO_2 eutectic ceramics fabricated via laser powder bed fusion, *J. Am. Ceram. Soc.*(2023), p. 1.

[26] Z. L. Shen, H. J. Su, H. F. Liu, D. Zhao, Y. Liu, Y. N. Guo, G. R. Fan, M. H. Yu, J. Chen, M. Guo, J. Zhang, L. Liu and H. Z. Fu, Directly fabricated Al_2O_3/$GdAlO_3$ eutectic ceramic with large smooth surface by selective laser melting: rapid solidification behavior and thermal field simulation, *J. Eur. Ceram. Soc.*, 42(2022), No.3, p. 1088.

[27] H. Liu, H. Su, Z. Shen, E. Wang, D. Zhao, M. Guo, J. Zhang, L. Liu and H. Fu, Direct formation of Al_2O_3/$GdAlO_3$/ZrO_2 ternary eutectic ceramics by selective laser melting: microstructure evolutions, *J. Eur. Ceram. Soc.*, 38(2018), No.15, p. 5144.

[28] V. K. Balla, S. Bose and A. Bandyopadhyay, Processing of bulk alumina ceramics using laser engineered net shaping, *Int. J. Appl. Ceram. Technol.*, 5(2008), No.3, p. 234.
[29] F. Niu, D. Wu, F. Lu, G. Liu, G. Ma and Z. Jia, Microstructure and macro properties of Al_2O_3 ceramics prepared by laser engineered net shaping, *Ceram. Int.*, 44(2018), No.12, p. 14303.
[30] Z. Fan, Y. Zhao, M. Lu and H. Huang, Yttria stabilized zirconia (YSZ) thin wall structures fabricated using laser engineered net shaping (LENS), *Int. J. Adv. Manuf. Technol.*, 105(2019), p. 4491.
[31] J. M. Pappas, A. R. Thakur, E. C. Kinzel and X. Dong, Direct 3D printing of transparent magnesium aluminate spinel ceramics, *J. Laser Appl.*, 33(2021), No.1, p. 012018.
[32] D. Wu, D. Zhao, Y. Huang, F. Niu and G. Ma, Shaping quality, microstructure, and mechanical properties of melt-grown mullite ceramics by directed laser deposition, *J. Alloy. Compd.*, 871(2021), p. 159609.
[33] F. Niu, D. Wu, G. Ma, J. Wang, M. Guo and B. Zhang, Nanosized microstructure of Al_2O_3-ZrO_2 (Y_2O_3) eutectics fabricated by laser engineered net shaping, *Scr. Mater.*, 95(2015), p. 39.
[34] Y. Hu, H. Wang, W. Cong and B. Zhao, Directed energy deposition of zirconia-toughened alumina ceramic: novel microstructure formation and mechanical performance, *J. Manuf. Sci. Eng.-Trans. ASME*, 142(2020), No.2, p. 021005.
[35] Z. Fan, Y. Yin, Q. Tan, X. Li, P. Niu, R. Li, T. Yuan, M.-X. Zhang and H. Huang, Unveiling solidification mode transition and crystallographic characteristics in laser 3D-printed Al_2O_3-ZrO_2 eutectic ceramics, *Scr. Mater.*, 210(2022), p. 114433.
[36] S. Yan, Y. Huang, D. Zhao, F. Niu, G. Ma and D. Wu, 3D printing of nano-scale Al_2O_3-ZrO_2 eutectic ceramic: principle analysis and process optimization of pores, *Addit. Manuf.*, 28(2019), p. 120.
[37] F. Li, X. Zhang, C. Sui, J. Wu, H. Wei and Y. Zhang, Microstructure and mechanical properties of Al_2O_3-ZrO_2 ceramic deposited by laser direct material deposition, *Ceram. Int.*, 44(2018), No.15, p. 18960.
[38] J. M. Pappas, A. R. Thakur and X. Dong, Effects of zirconia doping on additively manufactured alumina ceramics by laser direct deposition, *Mater. Des.*, 192(2020), p. 108711.

[39] Y. Huang, D. Wu, D. Zhao, F. Niu and G. Ma, Investigation of melt-growth alumina/aluminum titanate composite ceramics prepared by directed energy deposition, *Int. J. Extreme. Manuf.*, 3(2021), No.3, p. 035101.

[40] H. Su, H. Liu, H. Jiang, Z. Shen, Q. Chen, M. Yu, D. Zhao, X. Li, D. Dong and Z. Zhang, One-step preparation of melt-grown Al_2O_3/$GdAlO_3$/ZrO_2 eutectic ceramics with large size and irregular shape by directed energy deposition, *Addit. Manuf.*, 70(2023), p. 103563.

[41] Z. Fan, Y. Zhao, Q. Tan, N. Mo, M.-X. Zhang, M. Lu and H. Huang, Nanostructured Al_2O_3-YAG-ZrO_2 ternary eutectic components prepared by laser engineered net shaping, *Acta Mater.*, 170(2019), p. 24.

[42] Z. Fan, Y. Zhao, Q. Tan, B. Yu, M.-X. Zhang and H. Huang, New insights into the growth mechanism of 3D-printed Al_2O_3-$Y_3Al_5O_{12}$ binary eutectic composites, *Scr. Mater.*, 178(2020), p. 274.

[43] D. Zhao, D. J. Wu, J. Shi, F. Y. Niu and G. Y. Ma, Microstructure and mechanical properties of melt-grown alumina-mullite/glass composites fabricated by directed laser deposition, *J. Adv. Ceram.*, 11(2022), No.1, p. 75.

[44] I. Shishkovsky, I. Yadroitsev, P. Bertrand and I. Smurov, Alumina–zirconium ceramics synthesis by selective laser sintering/melting, *Appl. Surf. Sci.*, 254(2007), No.4, p. 966.

[45] A. Montón Zarazaga, M. Abdelmoula, G. Küçüktürk, F. Maury, M. Ferrato and D. Grossin, Process parameters investigation for direct powder bed selective laser processing of silicon carbide parts, *Prog. Addit. Manuf.*, 7(2022), No.6, p. 1307.

[46] Z. Shen, H. Su, M. Yu, Y. Guo, Y. Liu, D. Zhao, H. Jiang, P. Yang, M. Yang, Z. Zhang, M. Guo and W. Ren, Large-size complex-structure ternary eutectic ceramic fabricated using laser powder bed fusion assisted with finite element analysis, *Addit. Manuf.*, 72(2023), p. 103627.

[47] Y.-D. Qiu, J.-M. Wu, A.-N. Chen, P. Chen, Y. Yang, R.-Z. Liu, G. Chen, S. Chen, Y.-S. Shi and C.-H. Li, Balling phenomenon and cracks in alumina ceramics prepared by direct selective laser melting assisted with pressure treatment, *Ceram. Int.*, 46(2020), No.9, p. 13854.

[48] D. Wu, J. San, F. Niu, D. Zhao, X. Liang, S. Yan and G. Ma, Effect and mechanism of ZrO_2 doping on the cracking behavior of melt-grown Al_2O_3 ceramics prepared by directed laser deposition, *Int. J. Appl. Ceram. Technol.*, 17(2020), No.1, p. 227.

[49] Y. Huang, D. Wu, D. Zhao, F. Niu, H. Zhang, S. Yan and G. Ma, Process optimization of melt growth alumina/aluminum titanate composites directed energy deposition: effects of scanning speed, *Addit. Manuf.*, 35(2020), p. 101210.

[50] Y. Li, Y. Hu, W. Cong, L. Zhi and Z. Guo, Additive manufacturing of alumina using laser engineered net shaping: effects of deposition variables, *Ceram. Int.*, 43(2017), No.10, p. 7768.

[51] D. J. Wu, D. K. Zhao, F. Y. Niu, Y. F. Huang, J. Zhu and G. Y. Ma, In situ synthesis of melt-grown mullite ceramics using directed laser deposition, *J. Mater. Sci.*, 55(2020), No.27, p. 12761.

[52] J. C. Snyder and K. A. Thole, Understanding laser powder bed fusion surface roughness, *J. Manuf. Sci. Eng.-Trans. ASME*, 142(2020), No.7, p. 071003.

[53] F. Klocke and C. Ader, Direct laser sintering of ceramics, *International Solid Freeform Fabrication Symposium*, (2003), 447–455.

[54] Y. Tang, J. Y. H. Fuh, H. T. Loh, Y. S. Wong and L. Lu, Direct laser sintering of a silica sand, *Mater. Des.*, 24(2003), No.8, p. 623.

[55] Y. C. Hagedorn, N. Balachandran, W. Meiners, K. Wissenbach and R. Poprawe, SLM of net-shaped high strength ceramics: new opportunities for producing dental restorations, *International Solid Freeform Fabrication Symposium*, (2011), 8-10.

[56] M. Abdelmoula, G. Küçüktürk, E. Juste and F. Petit, Powder bed selective laser processing of alumina: scanning strategies investigation, *Appl. Sci.*, 12(2022), No.2, p. 764.

[57] Z. Xiong, K. Zhang, Z. Zhu, T. Liu, Y. Zhang, S. Li and W. Liao, Effect of laser focus shift on the forming quality, microstructure and mechanical properties of additively manufactured Al_2O_3-ZrO_2 eutectic ceramics, *Ceram. Int.*, 49(2023), No.22, p. 35948.

[58] Z. Xiong, K. Zhang, T. Liu, Z. Zhu, H. Wei, Z. Zou and W. Liao, Role of scanning speed on the microstructure and mechanical properties of additively manufactured Al_2O_3-ZrO_2, *J. Am. Ceram. Soc.*, 106(2023), No.12, p. 7760.

[59] G. K. Mishra, C. P. Paul, A. K. Rai, A. K. Agrawal, S. K. Rai and K. S. Bindra, Experimental investigation on laser directed energy deposition based additive manufacturing of Al_2O_3 bulk structures, *Ceram. Int.*, 47(2021), No.4, p. 5708.

[60] H. Liu, H. Su, Z. Shen, D. Zhao, Y. Liu, Y. Guo, J. Zhang, L. Liu and H. Fu, Insights into high thermal stability of laser additively manufactured

$Al_2O_3/GdAlO_3/ZrO_2$ eutectic ceramics under high temperatures, *Addit. Manuf.*, 48(2021), p. 102425.

[61] F. Y. Niu, D. J. Wu, S. Yan, G. Y. Ma and B. Zhang, Process optimization for suppressing cracks in laser engineered net shaping of Al_2O_3 ceramics, *JOM*, 69(2017), No.3, p. 557.

[62] Y. Zheng, K. Zhang, T. T. Liu, W. H. Liao, C. D. Zhang and H. Shao, Cracks of alumina ceramics by selective laser melting, *Ceram. Int.*, 45(2019), No.1, p. 175.

[63] H. Yves-Christian, W. Jan, M. Wilhelm, W. Konrad and P. Reinhart, Net shaped high performance oxide ceramic parts by selective laser melting, *Physics Procedia*, 5(2010), p. 587.

[64] J. Deckers, S. Meyers, J. P. Kruth and J. Vleugels, Direct selective laser sintering/melting of high density alumina powder layers at elevated temperatures, *Physics Procedia*, 56(2014), p. 117.

[65] Y. Huang, D. Wu, X. Yu, G. Ma, J. Han, H. Wang and F. Niu, Cracking mechanism in laser directed energy deposition of melt growth alumina/aluminum titanate ceramics, *J. Am. Ceram. Soc.*, 106(2023), No.7, p. 4358.

[66] Z. Liu, C. Ma, Z. Chang, P. Zhao, Y. Zhang, Q. Wu and F. Li, Formation mechanism and quantitative analysis of pores in Al_2O_3-ZrO_2 ceramic different structures by laser additive manufacturing, *Ceram. Int.*, 49(2023), No.10, p. 16099.

[67] F. Li, Z. Liu, B. Li, Y. Wang and Y. Zhang, Pore formation model for direct laser deposition of Al_2O_3-ZrO_2 ceramic, *J. Eur. Ceram. Soc.*, 42(2022), No.1, p. 207.

[68] B. Chang, C. Allen, J. Blackburn, P. Hilton and D. Du, Fluid flow characteristics and porosity behavior in full penetration laser welding of a titanium alloy, *Metall. Mater. Trans. B*, 46(2014), No.2, p. 906.

[69] Y. Wang, Q. Zhang, H. Zhang and J. Lei, Deep-learning-based localized porosity analysis for laser-sintered Al_2O_3 ceramic paste, *Ceram. Int.*, 49(2023), No.14, p. 23426.

[70] Q. Liu, Y. Danlos, B. Song, B. Zhang, S. Yin and H. Liao, Effect of high-temperature preheating on the selective laser melting of yttria-stabilized zirconia ceramic, *J. Mater. Process. Technol.*, 222(2015), p. 61.

[71] G. Ma, S. Yan, F. Niu, Y. Zhang and D. Wu, Microstructure and mechanical properties of solid Al_2O_3-ZrO_2 (Y_2O_3) eutectics prepared by laser engineered net shaping, *J. Laser Appl.*, 29(2017), No.2, p. 022305.

[72] S. Yan, D. Wu, F. Niu, Y. Huang, N. Liu and G. Ma, Effect of ultrasonic power on forming quality of nano-sized Al_2O_3-ZrO_2 eutectic ceramic via laser engineered net shaping (LENS), *Ceram. Int.*, 44(2018), No.1, p. 1120.

[73] Z. Liu, K. Song, B. Gao, T. Tian, H. Yang, X. Lin and W. Huang, Microstructure and mechanical properties of Al_2O_3/ZrO_2 directionally solidified eutectic ceramic prepared by laser 3D printing, *J. Mater. Sci. Technol.*, 32(2016), No.4, p. 320.

[74] S. Buls, J. Vleugels and B. Van Hooreweder, Microwave assisted selective laser melting of technical ceramics, *Annual international solid freeform fabrication symposium - an additive manufacturing conference*, (2018), 2349-2357.

[75] J. Wilkes, *Selective laser melting for generative production of components from high-strength oxide ceramics (in Germany)* [Dissertation], RWTH Aachen University, Aachen, Germany, 2009.

[76] Y. Hu, F. Ning, W. Cong, Y. Li, X. Wang and H. Wang, Ultrasonic vibration-assisted laser engineering net shaping of ZrO_2-Al_2O_3 bulk parts: effects on crack suppression, microstructure, and mechanical properties, *Ceram. Int.*, 44(2018), No.3, p. 2752.

[77] D. Wu, F. Lu, D. Zhao, G. Ma, C. Li, J. Ding and F. Niu, Effect of doping SiC particles on cracks and pores of Al_2O_3-ZrO_2 eutectic ceramics fabricated by directed laser deposition, *J. Mater. Sci.*, 54(2019), No.13, p. 9321.

[78] S. Yan, D. Wu, Y. Huang, N. Liu, Y. Zhang, F. Niu and G. Ma, C fiber toughening Al_2O_3-ZrO_2 eutectic via ultrasonic-assisted directed laser deposition, *Mater. Lett.*, 235(2019), p. 228.

[79] S. Pfeiffer, K. Florio, M. Makowska, C. G. Aneziris, H. Van Swygenhoven, K. Wegener and T. Graule, Crack-reduced laser powder bed fused oxide ceramic parts by in-situ synthesis of negative thermal expansion phases, *J. Eur. Ceram. Soc.*, 44(2024), No.2, p. 1012.

[80] H. F. Liu, H. J. Su, Z. L. Shen, D. Zhao, Y. Liu, Y. N. Guo, H. T. Guo, M. Guo, K. Y. Xie, J. Zhang, L. Liu and H. Z. Fu, One-step additive manufacturing and microstructure evolution of melt-grown Al_2O_3/$GdAlO_3$/ZrO_2 eutectic ceramics by laser directed energy deposition, *J. Eur. Ceram. Soc.*, 41(2021), No.6, p. 3547.

[81] S. Pfeiffer, M. Makowska, K. Florio, D. F. Sanchez, F. Marone, X. Zhang, C. G. Aneziris, H. Van Swygenhoven, K. Wegener and T. Graule, Selective laser melting of thermal pre-treated metal oxide doped aluminum oxide granules, *Open Ceram.*, 2(2020), p. 100007.

[82] J. M. Pappas and X. Dong, Effects of processing conditions on laser direct deposited alumina ceramics, *International Manufacturing Science and Engineering Conference*, 84256, (2020), V001T001A002.
[83] Y. Waku, N. Nakagawa, T. Wakamoto, H. Ohtsubo, K. Shimizu and Y. Kohtoku, A ductile ceramic eutectic composite with high at 1873 K, *Nature*, 389(1997), No.6646, p. 49.
[84] S. Yan, D. Wu, G. Ma, F. Niu, R. Kang and D. Guo, Formation mechanism and process optimization of nano Al_2O_3-ZrO_2 eutectic ceramic via laser engineered net shaping (LENS), *Ceram. Int.*, 43(2017), No.17, p. 14742.
[85] H. Z. Fu, J. J. Guo, L. Liu and I. S. Li, *Directional solidification and processing of advanced materials (in chinese)*, Science Press, Beijing, 2008.
[86] F. Niu, D. Wu, G. Ma, S. Zhou and B. Zhang, Effect of second-phase doping on laser deposited Al_2O_3 ceramics, *Rapid Prototyping J.*, 21(2015), No.2, p. 201.
[87] D. Wu, H. Liu, F. Lu, G. Ma, S. Yan, F. Niu and D. Guo, Al_2O_3-YAG eutectic ceramic prepared by laser additive manufacturing with water-cooled substrate, *Ceram. Int.*, 45(2019), No.3, p. 4119.
[88] H. F. Liu, H. J. Su, Z. L. Shen, D. Zhao, Y. Liu, Y. N. Guo, M. Guo, J. Zhang, L. Liu and H. Z. Fu, Preparation of large-size Al_2O_3/$GdAlO_3$/ZrO_2 ternary eutectic ceramic rod by laser directed energy deposition and its microstructure homogenization mechanism, *J. Mater. Sci. Technol.*, 85(2021), p. 218.
[89] D. J. Wu, Y. F. Huang, F. Y. Niu, G. Y. Ma, S. Yan, C. J. Li and J. Din, Effects of TiO_2 doping on microstructure and properties of directed laser deposition alumina/aluminum titanate composites, *Virtual Phys. Prototy.*, 14(2019), No.4, p. 371.
[90] A. Montón, M. Abdelmoula, G. Küçüktürk, F. Maury, D. Grossin and M. Ferrato, Experimental and numerical study for direct powder bed selective laser processing (sintering/melting) of silicon carbide ceramic, *Mater. Res. Express*, 8(2021), No.4, p. 045603.
[91] D. J. Wu, J. D. San, F. Y. Niu, D. K. Zhao, Y. F. Huang and G. Y. Ma, Directed laser deposition of Al_2O_3-ZrO_2 melt-grown composite ceramics with multiple composition ratios, *Journal of Materials Science*, 55(2020), No.16, p.
[92] S. Yan, D. Wu, F. Niu, G. Ma and R. Kang, Al_2O_3-ZrO_2 eutectic ceramic via ultrasonic-assisted laser engineered net shaping, *Ceram. Int.*, 43(2017), No.17, p. 15905.

[93] D. Zhao, G. Bi, J. Chen, J. Zhu, F. Niu, G. Ma and D. Wu, Melt-grown behaviour of heat treated high-purity alumina ceramics prepared by laser directed energy deposition, *Ceram. Int.*, 50(2024), No.1, p. 1777.
[94] D. Zhao, D. Wu, F. Niu, Y. Huang, G. Ma, C. Zhou, B. Zhang and G. Ren, Heat treatment of melt-grown alumina ceramics with trace glass fabricated by laser directed energy deposition, *Mater. Charact.*, 196(2023), p. 112639.
[95] F. Verga, M. Makowska, G. Cellerai, K. Florio, M. Schmid and K. Wegener, Crack-healing, a novel approach for a laser-based powder bed fusion of high-performance ceramic oxides, *Addit. Manuf. Lett.*, 1(2021), p. 100021.
[96] H. F. Liu, H. J. Su, Z. L. Shen, H. Jiang, D. Zhao, Y. Liu, Y. N. Guo, X. Li, M. Guo, J. Zhang, L. Liu and H. Z. Fu, Formation mechanism and roles of oxygen vacancies in melt-grown $Al_2O_3/GdAlO_3/ZrO_2$ eutectic ceramic by laser 3D printing, *J. Adv. Ceram.*, 11(2022), No.11, p. 1751.
[97] M. Wang, S. Shi and J. Fineberg, Tensile cracks can shatter classical speed limits, *Science*, 381(2023), No.6656, p. 415.
[98] E. L. Pang, G. B. Olson and C. A. Schuh, Low-hysteresis shape-memory ceramics designed by multimode modelling, *Nat. Commun.*, 610(2022), No.7932, p. 491.